International Journal of Solids and Structures 51 (2014) 575–598

Contents lists available at ScienceDirect

International Journal of Solids and Structures

journal homepage: www.elsevier.com/locate/ijsolstr

A higher order model for thin-walled structures with deformable cross-sections

R.F. Vieira *, F.B. Virtuoso, E.B.R. Pereira

Universidade de Lisboa, Instituto Superior Técnico, Department of Civil Engineering, Architecture and Georesources, Av. Rovisco Pais, 1049-001 Lisboa, Portugal

ARTICLE INFO

Article history:
Received 22 November 2012
Received in revised form 14 October 2013
Available online 26 October 2013

Keywords:
Thin-walled structures
Higher order deformation modes
Warping
Distortion

ABSTRACT

A higher order model for the analysis of linear, prismatic thin-walled structures that considers the cross-section warping together with the cross-section in-plane flexural deformation is presented in this paper. The use of a one-dimentional model for the analysis of thin-walled structures, which have an inherent complex three-dimensional (3D) behaviour, can only be successful and competitive when compared with shell finite element models if it fulfills a twofold objective: (i) an enrichment of the model in order to as accurately as possible reproduce its 3D elasticity equations and (ii) the definition of a consistent criterion for uncoupling the beam equations, allowing to identify structural deformation modes.

The displacement field is approximated through a linear combination of products between a set of linear independent functions defined over the cross-section and the associated weights only dependent on the beam axis; this approximation is not constrained by any *ab initio* kinematic assumptions. Towards an efficient application of the approximation procedure, the cross-section is discretized into thin-walled elements, being the displacement field approximated for each element independently of the displacement direction. The approximation is thus *hp* refined enhancing the "capture" of the 3D structural mechanics of thin-walled structures. The beam model governing equations are obtained through the integration over the cross-section of the corresponding elasticity equations weighted by the cross-section global approximation functions.

A criterion for uncoupling the beam governing equations is established, allowing to (i) retrieve the classic equations of the thin-walled beam theory both for open and closed sections and (ii) derive a set of uncoupled deformation modes representing higher order effects. The criterion is based on the solution of the polynomial eigenvalue problem associated with the beam differential equations, allowing to quantify the Saint-Venant principle for thin-walled structures. In fact, the solution of the non linear eigenvalue problem yields a twelve fold null eigenvalue (representing polynomial solutions) that are verified to represent beam classic solutions and sets of pairs and quadruplets of non-null eigenvalues corresponding to higher order modes of deformation.

1. Introduction

The analysis of prismatic thin-walled structures through one-dimensional models represents a simple and efficient procedure that has been successfully adopted. This trend of analysis has evolved through the development of refined beam models in order to represent the corresponding three-dimensional structural behaviour side by side with the deployment of an increasingly enhanced technology of shell finite elements available to model such structures.

However, the use of shell finite elements, although being inherently accurate in modelling the 3D structural behaviour of thin-walled structures, is not only costly in terms of computing resources, but also presents a cumbersome set of results that can difficult the interpretation of the relevant phenomena from less experienced users. Moreover, the modelling by shell finite elements requires a significant amount of data that remains unknown at a preliminary stage of design, being also more prone to modelling errors from users when compared with beam models.

The formulation of beam models by reducing the 3D elasticity formulation to a one-dimensional model must be as accurate as possible in order to include the most significative structural phenomena. Towards this end, several trends of enhancing beam theories are identified: asymptotical methods, in particular variational asymptotical beam sectional analysis (VABS) by Yu et al. (2012), expansion of the beam displacement field through Taylor series (Carrera and Giunta, 2010; Carrera et al., 2011; Carrera and Petrolo, 2011, Saint-Venant driven models (Toupin, 1965; Knowles, 1966; Cowper, 1966; Horgan, 1989; Giavotto et al., 1983; Bauchau,

* Corresponding author.
E-mail address: ricardo.figueiredo.vieira@ist.utl.pt (R.F. Vieira).

0020-7683/$ - see front matter © 2013 Elsevier Ltd. All rights reserved.
http://dx.doi.org/10.1016/j.ijsolstr.2013.10.023

1985; Laudiero and Savoia, 1990; Rubin, 2003; Ladevèze et al., 2003; Fatmi, 2007; Morandinia et al., 2010) and refinement of the classic thin-walled theory which was cast through the seminal works of Umansky (1940), von Kármán and Christensen (1944), Flügge and Marguerre (1948) and Vlassov (1961) towards the consideration of the cross-section in-plane deformation and additional degrees of warping (Bazant, 1968; Bazant and El Nimieri, 1974) and "additional" deformations modes in order to combine the warping due to torsion and related with shear-lag effects together with the cross-section deformation flexure (Mikkola and Paavola, 1980; Paavola, 1990; Tesar, 1996; Razaqpur and Li, 1991, 1994; Prokic, 1996a,b, 2002 and Kim and Kim, 1999a,b, 2000, 2002, 2003).

Some other formulations stemming from the classic thin-walled beam theory have been developed by considering the addition of "representative" deformation modes that were obtained through simplified models that are often thought for specific structural behaviours and/or load conditions. The analysis of the cross-section distortion in box girders through an analogy of a beam on an elastic foundation is a successful example of these models, Wright and Abdel-Samad (1968) and Hsu (1995) as well as the analysis of the distortion presented in Boswell and Zhang (1984) and Kermani and Waldron (1993) and more recently solutions for multi-cell distortion given by Pavazza (2002), Pavazza and Blagojević, 2005 and Park et al. (2005); and the warping due to the shear-lag effects (Kuzmanovic and Graham, 1981; Foutch and Chang, 1982 and Dezi and Mentrasti, 1985). The in-plane distortion of thin-walled structures has been also was considered through the definition of distortional modes (Saadé et al., 2006).

A beam theory that considers both the warping and the cross-section distortion, allowing to derive a set of the corresponding modes is the generalised beam theory (GBT) that since its inception in Schardt (1966) and Schardt (1989) has been subjected to several developments. In fact, Initially, the theory did not allow to consider multi-cell closed cross-sections and open cross-sections with more than two walls converging in a node, which has been coped through new formulations by Möller (1982), Simão (2005) and Gonçalves (2007) and more recently to arbitrary sections in Dinis et al. (2006), Gonçalves et al. (2009) and Gonçalves et al. (2010). The theory has also been developed to account for shear deformation and transverse extension, being also applied to composite materials in Silvestre and Camotim (2002a) and Silvestre and Camotim (2002b).

A definition of the distortional displacement field within the framework of GBT has been presented and applied in Jönsson and Andreassen (2011, 2012) and Andreassen and Jönsson (2013). This novel approach considers a cross-section discretization into elements, which includes rotational degrees of freedom for the transverse displacements perpendicular to the wall, and from an approximation similar to the GBT formulations establishes a governing equation for the beam model. The displacement field displacement approximation considers the amplitude of the warping displacement shape functions to be the derivative of the transverse displacement amplitudes. This fact together with shear constraints allowed to bind together axial and transverse displacements, which was adopted for the definition of warping functions from the transverse displacements and for rewriting the beam governing equations in terms of transverse displacements.

The formulation considers a strategy of eliminating classic solutions (axial pure modes, translational modes and rotational modes) from the beam governing equations in order to derive a set of equations that defines distortional behaviour. The pure axial extension is identified as a solution of the equations and a linear solution is put forward since the amplitude for the axial mode is admitted to correspond to the derivative of the transverse displacements. Despite referring to the pure axial mode as an eigenmode solution, no statement of the corresponding eigenvalue is presented and hence the corresponding polynomial solution considered does not identify the respective generalised eigenvectors. By eliminating the axial mode, the set of beam equations is written in terms of transverse displacements, which is adopted to identify the transverse rigid cross-section translations and the pure rotational mode. The translational modes are obtained from the eigenvectors of a standard eigenvalue problem applied to the axial stiffness matrix, being the rotational mode defined by requiring that the coupling terms in the axial stiffness cancel. Furthermore, the membrane tangential displacements along each wall element are set to be equal so as to enforce the transverse strain of the middle surface null. The beam equations are rewritten for a new set of coordinates that consider the translational modes, the rotational modes and the tangential constraint, being tested a polynomial cubic solution for the translational modes.

The procedure adopted for identifying and in the sequel eliminate the so-called axial, translational and rotational modes is quite different from that applied in Vieira et al. (2013). In fact, the classic solutions of beam theory, including shear effects, are obtained through the eigenvectors and generalised eigenvectors associated with a 12-fold null eigenvalue, which is a solution of the non-linear eigenvalue associated with the beam model differential equations. Moreover, the correct procedure for eliminating these classic modes from higher order modes is essential to obtain an isospectral transformation of modes.

On the other hand, the GBT formulation of Jönsson and Andreassen (2011) considers a different strategy for identifying the classic modes. In fact, the null eigenvalue is identified as the solution associated with classic modes, but the polynomial solutions put forward for each of the classic modes are not demonstrated to correspond to the respective generalized eigenvectors: As a result the solution lacks of consistency insofar as the corresponding algebraic and geometric multiplicities do not coincide. In fact, in the examples presented in Jönsson and Andreassen (2011) the classic modes are associated with a null eigenvalue with an algebraic multiplicity of 8, despite having a 12-fold geometric multiplicity. In the proposed higher order model the classic solution stems directly from the computation of the Jordan chain associated with a 12-fold null eigenvalue, clearly identifying extension, flexure (with and without shear) and torsion classic structural behaviour, but also rigid body motions.

A semi-analytical finite strip analysis (the constrained finite strip analysis – cFSM) has been able to shed a light regarding the mechanical behaviour of thin-walled structures through the separation of the corresponding deformation modes (Li et al., 2011; Ádány and Schafer, 2008). A comparison between the modal approaches between GBT and is cFSM has been presented in Ádány et al. (2009).

A one-dimensional model for the three-dimensional structural analysis of prismatic thin-walled structures with an arbitrary midline geometry considering the cross-section warping together with its transverse deformation is presented in this paper. This higher order model represents a novel beam formulation capable of representing the three-dimensional structural behaviour of thin-walled structures, being an alternative to other theories such as those of Pavazza and Blagojević (2005), Dinis et al. (2006), Saadé et al. (2006), Gonçalves et al. (2010) and Carrera and Giunta (2010). The beam model is thought to be cast within the framework of the finite element method and derived in a unified formulation (i.e. the formulation is independent of the cross-section type).

A previous papers by the authors (Vieira et al., 2013) considers the cross-section in-plane undeformable in order to obtain a set of warping and shear modes. A more general formulation including in-plane deformation is now proposed with a particular focus on the definition of uncoupled modes. The uncoupling procedure is derived from a quartic eigenvalue problem, which given its

Hamiltonian structure implies a spectrum with pairs of symmetric real eigenvalues and quadruples of symmetric conjugate eigenvalues.

Towards the definition of a numerical model as accurate as possible, it was considered essential that the model formulation should: (i) allow to recover classic solutions (including the effect of shear deformation); consider an unrestricted approximation of the displacement field, being adaptive towards the enhancement of the solution; (ii) define a set of uncoupled deformation modes obtained from a unique and consistent criterion, being applicable to any cross-section geometry; (iii) consider a consistent criterion for an hierarchical selection of modes.

The model considers a projection of the displacement field on the beam cross-section through a set of linear independent basis functions (this formulation could thus be labelled a beam projection theory, according to Antman (1984) in relation to the classification of beam theories). The basis functions adopted are polynomials, of an arbitrary degree, defined over the beam cross-section, guaranteeing the compatibility of the displacement field along the thin-walled cross-section midline. The projection of the displacement field can be defined globally, in the sense that the interpolation functions can be defined over the beam cross-section taken as a whole. However, it is more efficient to consider the cross-section to be constituted by an assemblage of thin-walled laminar elements and consider the approximation of the displacement field in each element.

This approximation of the displacement field is independent of the structural behaviour of the cross-section, only carrying a kinematical nature (aims at an interpolation of displacements), being the deformation modes derived from the beam governing solutions, in particular through the corresponding non-linear eigenvalue problem. Regarding the approximation scheme, it should be mentioned that approximations of the same type have already been adopted by Jönsson and Andreassen (2011), Haakh (2004) and Möller (1982).

A suitable mesh of cross-section elements is then adopted for the cross-section analysis, being the elements assembled by verifying the compatibility conditions between the corresponding boundaries. Therefore, the model can cope with the loss of accuracy inherent from the reduction of a three dimensional elasticity formulation to a one-dimensional model by an enrichment of the beam displacement field on the beam cross-section through the adoption of a set of interpolation functions of a suitable degree, defined over a sufficiently refined mesh of the cross-section.

The beam governing equations are derived considering the approximation scheme adopted for the displacement, yielding a set of fourth order differential system of equations. The solution of this system is analyzed through the corresponding non linear eigenvalue problem, which is obtained by admitting an exponential solution of the problem. A twelve fold null eigenvalue is obtained, which being solved through a Jordan chain of matrices allow to retrieve classic solutions by the associated generalized eigenvectors. A set of non null eigenvalue are obtained, where the corresponding eigenvectors define uncoupled deformation modes. The real part of the non null eigenvalue allows to establish an hierarchical selection of modes inasmuch it represents the inverse of the decay length. A set of displacement modes is obtained from the generalized eigenvectors and the higher order deformation modes allowing to rewrite the beam governing equations in a new system of coordinates in an uncoupled form and with a structural interpretation.

2. Beam model formulation

The cross-section layout considered in this formulation is constituted by a set of rectilinear wall segments (thin-walled laminar elements) forming a generic shape, either of open or closed profile. A rectilinear segment can be divided into elements for better approximation features. Each laminar element is considered to have both a flexural and a membrane structural behaviour. For the flexural behaviour, it is assumed that the elements are sufficiently "thin" in order to consider valid the *Kirchhoff* formulation and hence neglect the shear deformation on the planes perpendicular to the middle surface.

The displacement field considering both the membrane and the flexural structural behaviour of the plate is defined as follows:

$$u_x(x,s,n) = u_x(x,s) - n\frac{\partial u_n}{\partial x}, \quad u_s(x,s,n) = u_s(x,s) - n\frac{\partial u_n}{\partial s} \quad \text{and} \quad u_n(x,s,n) = u_n(x,s) \tag{1}$$

where x represents the beam axis; s the coordinate along the cross-section profile and n the corresponding perpendicular; $u_x(x,s)$ and $u_s(x,s)$ represent the in-plane displacements associated with the plate membrane behaviour and $u_n(x,s,n)$, the plate transverse displacement, which is considered to be constant over the plate element thickness.

The displacement field variables $u_x(x,s), u_s(x,s)$ and $u_n(x,s)$, defined on the plate element middle surface, are independently approximated through a set of linear independent basis functions defined along the coordinate s. This approximation has inherently the virtue of separating the variable dependencies on the x and the s dimension, being interpreted as a projection of the displacement field variables into a reference system defined by the selected basis functions (Antman, 1984).

The displacement field of the cross-section middle surface is thus approximated in the three spatial directions, as in the work of Möller (1982), through the following expression,

$$u_x(x,s) = \boldsymbol{\phi}^t \mathbf{u}_x, \quad u_s(x,s) = \boldsymbol{\psi}^t \mathbf{u}_s \quad \text{and} \quad u_n(x,s) = \boldsymbol{\chi}^t \mathbf{u}_n \tag{2}$$

where $\boldsymbol{\phi}, \boldsymbol{\psi}$ and $\boldsymbol{\chi}$ correspond to the sets of the adopted basis functions; each set of basis functions is constituted by linearly independent functions defined on the beam cross-section that guarantee the continuity of the displacement field along the cross-section midline profile.

A complete kinematical description for the thin-walled structure is obtained by substituting the approximations made in Eq. (2) into the displacement field definition given by Eq. (1), being written as follows:

$$u_x(x,s) = \boldsymbol{\phi}^t \mathbf{u}_x - n\,\boldsymbol{\chi}^t \mathbf{u}_n' \tag{3}$$

$$u_s(x,s) = \boldsymbol{\psi}^t \mathbf{u}_s - n\,\boldsymbol{\chi}_{,s}^t \mathbf{u}_n \tag{4}$$

$$u_n(x,s) = \boldsymbol{\chi}^t \mathbf{u}_n \tag{5}$$

where the prime following a vector represents the derivative of the corresponding components in the axial direction (d/dx) and the vector subscript $(,s)$ stands for the component derivatives in the variable s.

The deformation field is obtained under the small displacements hypothesis through the Cauchy infinitesimal compatibility operator, which for the deformation components of the *Kirchhoff* formulation is written as follows,

$$\boldsymbol{\epsilon} = \mathbb{D}_k^* \mathbf{u} \quad \text{with} \quad \boldsymbol{\epsilon} = [\epsilon_x(x,s,n) \quad \epsilon_s(x,s,n) \quad \gamma_{xs}(x,s,n)]^t \tag{6}$$

being the compatibility operator given by:

$$\mathbb{D}_k^* = \begin{bmatrix} \frac{\partial}{\partial x} & \cdot & \cdot \\ \cdot & \frac{\partial}{\partial s} & \cdot \\ \frac{\partial}{\partial s} & \cdot & \frac{\partial}{\partial x} \end{bmatrix} \tag{7}$$

Taking in account the displacement field approximation obtained through (2) and the compatibility condition (6) the deformation components would read as follows,

$$\epsilon_x(x,s,n) = \boldsymbol{\phi}^t \mathbf{u}'_x - n\,\boldsymbol{\chi}^t \mathbf{u}''_n \tag{8}$$

$$\epsilon_s(x,s,n) = \boldsymbol{\psi}^t_{,s} \mathbf{u}_s - n\,\boldsymbol{\chi}^t_{,ss} \mathbf{u}_n \tag{9}$$

$$\gamma_{xs}(x,s,n) = \boldsymbol{\psi}^t \mathbf{u}'_s + \boldsymbol{\phi}^t_{,s} \mathbf{u}_x - 2n\,\boldsymbol{\chi}^t_{,s} \mathbf{u}'_n \tag{10}$$

The corresponding stress field can be obtained through the constitutive relation,

$$\boldsymbol{\sigma} = \mathbf{C}\boldsymbol{\epsilon} \quad \text{with} \quad \boldsymbol{\sigma} = [\sigma_x(x,s,n) \quad \sigma_s(x,s,n) \quad \sigma_{xs}(x,s,n)]^t \tag{11}$$

where the constitutive matrix $\mathbf{C}$ is defined for a plane stress of each wall considering a plate flexural behaviour.

The stress field is obtained through Eq. (11) by taking in account the constitutive relation (11) and the strain field given by Eqs. (8)–(10), being written in terms of the displacement field as follows,

$$\sigma_x(x,s,n) = E^*\left(\boldsymbol{\phi}^t \mathbf{u}'_x + \nu \boldsymbol{\psi}^t_{,s} \mathbf{u}_s\right) - nE^*\left(\boldsymbol{\chi}^t \mathbf{u}''_n + \nu\, \boldsymbol{\chi}^t_{,ss} \mathbf{u}_n\right) \tag{12}$$

$$\sigma_s(x,s,n) = E^*\left(\boldsymbol{\psi}^t_{,s} \mathbf{u}_s + \nu\, \boldsymbol{\phi}^t \mathbf{u}'_x\right) - nE^*\left(\boldsymbol{\chi}^t_{,ss} \mathbf{u}_n + \nu\, \boldsymbol{\chi}^t \mathbf{u}''_n\right) \tag{13}$$

$$\sigma_{xs}(x,s,n) = G\left(\boldsymbol{\psi}^t \mathbf{u}'_s + \boldsymbol{\phi}^t_{,s} \mathbf{u}_x\right) - 2nG\,\boldsymbol{\chi}^t_{,s} \mathbf{u}'_n \tag{14}$$

being E and ν the elasticity modulus and the *Poisson* coefficient, respectively.

In terms of applied loads, the thin-walled beam is admitted to be subjected to a set of distributed forces along the axis and to a set of tractions applied at both beam end sections. The distributed forces are defined by a set of vectors that gather the corresponding densities defined on the thin-walled middle surface (x,s), which is written as,

$$\mathbf{f} = [f_x(x,s) \quad f_s(x,s) \quad f_n(x,s)]^t \tag{15}$$

where $f_x(x,s), f_s(x,s)$ and $f_n(x,s)$ represent the force densities along directions x, s and n, respectively.

The forces applied to the beam model are obtained by integrating the density forces (15) over the thin-walled cross-section by adopting for weights the displacement field approximation. The vector of generalised forces distributed along the beam axis is then written as follows,

$$\mathbf{p} = [\mathbf{p}_x(x) \quad \mathbf{p}_s(x) \quad \mathbf{p}_n(x)]^t \tag{16}$$

where the corresponding components are given by,

$$\begin{aligned}\mathbf{p}_x(x) &= \int_\Gamma \boldsymbol{\phi} f_x(x,s)\,d\Gamma \quad \mathbf{p}_s(x) = \int_\Gamma \boldsymbol{\psi} f_s(x,s)\,d\Gamma \quad \mathbf{p}_n(x) \\ &= \int_\Gamma \left[\boldsymbol{\chi} f_n(x,s) - \frac{\partial \tilde{m}_{xs}}{\partial s} - \frac{\partial \tilde{m}_x}{\partial x}\right] d\Gamma\end{aligned} \tag{17}$$

being $\tilde{m}_{xs}$ and $\tilde{m}_{xs}$ the distributed moments given by,

$$\tilde{m}_{xs} = -n\,\boldsymbol{\chi}_{,s} f_s \quad \text{and} \quad \tilde{m}_x = -n\,\boldsymbol{\chi} f_x$$

A set of generalized end forces are obtained by integrating over the cross-section the tractions applied at the end sections, $\hat{\mathbf{t}}$, weighted by the respective displacement field approximation functions, being given as follows:

$$\hat{\mathbf{Q}} = \left[\hat{\mathbf{Q}}_x \quad \hat{\mathbf{Q}}_s \quad \hat{\mathbf{Q}}_n\right]^t \quad \text{with} \tag{18}$$

$$\begin{aligned}\hat{\mathbf{Q}}_x &= \int_{\hat{\Gamma}} \boldsymbol{\phi}\, \hat{t}_x(s)\,d\Gamma \quad \hat{\mathbf{Q}}_s = \int_{\hat{\Gamma}} \boldsymbol{\psi}\, \hat{t}_s(s)\,d\Gamma \\ \hat{\mathbf{Q}}_n &= \int_{\hat{\Gamma}} \left[\boldsymbol{\chi}\, \hat{t}_n(s) - \frac{\partial \tilde{m}_{xs}}{\partial s} - \frac{\partial \tilde{m}_x}{\partial x}\right] d\Gamma\end{aligned}$$

where $\hat{\Gamma}$ represent the contour of the cross-section midline profile at the end section, being the prescribed tractions defined as follows,

$$\hat{\mathbf{t}} = \left[\hat{t}_x(s) \quad \hat{t}_s(s) \quad \hat{t}_n(s)\right]^t \tag{19}$$

The beam total energy is a functional of the beam displacement field coordinates and its respective derivatives, being given through the following expression,

$$\mathscr{V} = \frac{1}{2}\int_\Omega \boldsymbol{\sigma}^t \boldsymbol{\epsilon}\, d\Omega - \int_0^L \mathbf{p}^t \mathbf{u}\, dx - \left[\hat{\mathbf{Q}}^t \mathbf{u}\right]_{\hat{\Gamma}} \tag{20}$$

where the following definition applies: L, the beam length; Γ, the cross-section and Ω the volume of the thin-walled beam, which is formally defined by:

$$\Omega = \{(x,s,n) \in \mathbb{R}^3 \,|\, x \in [0 \quad L], \quad s \in \Gamma \quad \wedge \quad n \in [-t/2 \quad t/2]\} \tag{21}$$

The first variation of the thin-walled energy on a virtual displacement field $\delta\mathbf{u}$, and otherwise kinematical admissible, submitted to a set of lengthwise distributed forces, $\mathbf{p}$, and to the concentrated forces applied at the end sections, $\mathbf{Q}$, is written as follows:

$$\delta\mathscr{V} = \delta U_x + \delta U_s + \delta U_{xs} - \int_0^L \mathbf{p}^t \delta\mathbf{u}\, dx - \left[\hat{\mathbf{Q}}^t \delta\mathbf{u}\right]_{\hat{\Gamma}} \tag{22}$$

being the terms $\delta U_x, \delta U_s$ and δU_{xs}, the deformation energy associated with the stress fields σ_x, σ_s and σ_{xs}, respectively, which are obtained by:

$$\delta U_x = \int_\Omega \sigma_x \delta\epsilon_x\, d\Omega \quad \delta U_s = \int_\Omega \sigma_s \delta\epsilon_s\, d\Omega \quad \delta U_{xs} = \int_\Omega \sigma_{xs} \delta\gamma_{xs}\, d\Omega \tag{23}$$

where the deformation variations $\delta\epsilon_x, \delta\epsilon_s$ and $\delta\gamma_{xs}$ are defined by the variation of the deformation components given by (8)–(10), respectively.

The variation of the total energy defined in Eq. (22) is derived in order to establish the thin-walled equilibrium equations, being presented in the sequel analysing in separate each functional term. The deformation terms $\delta U_x, \delta U_s$ and δU_{xs} are written considering the stress field defined in Eqs. (12)–(14) as follows:

$$\delta U_x[\mathbf{u}''_n, \mathbf{u}'_x, \mathbf{u}_s, \mathbf{u}_n, \delta\mathbf{u}''_n, \delta\mathbf{u}'_x] = \delta U_x = \delta U^a_x + \delta U^b_x + \delta U^c_x + \delta U^d_x \tag{24}$$

where $\delta U^a_x, \delta U^b_x, \delta U^c_x, \delta U^d_x$ are defined as follows:

$$\begin{aligned}\delta U^a_x &= E^* t \int_0^L \int_\Gamma (\boldsymbol{\phi}^t \mathbf{u}'_x)(\boldsymbol{\phi}^t \delta\mathbf{u}'_x)\, d\Gamma\, dx \\ \delta U^b_x &= E^* \nu t \int_0^L \int_\Gamma \left(\boldsymbol{\psi}^t_{,s} \mathbf{u}_s\right)(\boldsymbol{\phi}^t \delta\mathbf{u}'_x)\, d\Gamma\, dx \\ \delta U^c_x &= \frac{E^* t^3}{12} \int_0^L \int_\Gamma (\boldsymbol{\chi}^t \mathbf{u}''_n)(\boldsymbol{\chi}^t \delta\mathbf{u}''_n)\, d\Gamma\, dx \\ \delta U^d_x &= \frac{E^* \nu t^3}{12} \int_0^L \int_\Gamma \left(\boldsymbol{\chi}^t_{,ss} \mathbf{u}_n\right)(\boldsymbol{\chi}^t \delta\mathbf{u}''_n)\, d\Gamma\, dx\end{aligned} \tag{25, 26}$$

where the deformation functional terms δU^a_x and δU^b_x, which correspond to the membrane structural behaviour, have to be integrated by parts in relation to $\delta\mathbf{u}'_x$, whereas the terms δU^c_x and δU^d_x, which represent the flexural structural behaviour, must be integrated twice by parts relatively to $\delta\mathbf{u}''_n$ due to the *Kirchhoff* formulation.

$$\delta U_s[\mathbf{u}''_n, \mathbf{u}'_x, \mathbf{u}_s, \mathbf{u}_n, \delta\mathbf{u}_n, \delta\mathbf{u}_s] = \delta U^a_s + \delta U^b_s + \delta U^c_s + \delta U^d_s \tag{27}$$

where $\delta U^a_s, \delta U^b_s, \delta U^c_s$ and δU^d_s correspond to the following expressions,

$$\delta U_s^a = E^* t \int_0^L \int_\Gamma \left(\boldsymbol{\psi}_{,s}^t \mathbf{u}_s\right)\left(\boldsymbol{\psi}_{,s}^t \delta\mathbf{u}_s\right) d\Gamma\, dx$$
$$\delta U_s^b = E^* \nu t \int_0^L \int_\Gamma \left(\boldsymbol{\phi}^t \mathbf{u}_x'\right)\left(\boldsymbol{\psi}_{,s}^t \delta\mathbf{u}_s\right) d\Gamma\, dx \tag{28}$$
$$\delta U_s^c = \frac{E^* t^3}{12} \int_0^L \int_\Gamma \left(\boldsymbol{\chi}_{,ss}^t \mathbf{u}_n\right)\left(\boldsymbol{\chi}_{,ss}^t \delta\mathbf{u}_n\right) d\Gamma\, dx$$
$$\delta U_s^d = \frac{E^* \nu t^3}{12} \int_0^L \int_\Gamma \left(\boldsymbol{\chi}^t \mathbf{u}_n''\right)\left(\boldsymbol{\chi}_{,ss}^t \delta\mathbf{u}_n\right) d\Gamma\, dx \tag{29}$$

$$\delta U_{xs}\left[\mathbf{u}_n'', \mathbf{u}_x', \mathbf{u}_s, \mathbf{u}_n, \delta\mathbf{u}_n'', \delta\mathbf{u}_x'\right] = \delta U_{xs} = \delta U_{xs}^a + \delta U_{xs}^b + \delta U_{xs}^c + \delta U_{xs}^d + \delta U_{xs}^e \tag{30}$$

where the terms $\delta U_{xs}^a, \delta U_{xs}^b, \delta U_{xs}^c, \delta U_{xs}^d$ and δU_{xs}^e are given by:

$$\delta U_{xs}^a = G t \int_0^L \int_\Gamma \left(\boldsymbol{\phi}_{,s}^t \mathbf{u}_x\right)\left(\boldsymbol{\phi}_{,s}^t \delta\mathbf{u}_x\right) d\Gamma\, dx$$
$$\delta U_{xs}^b = G t \int_0^L \int_\Gamma \left(\boldsymbol{\phi}_{,s}^t \mathbf{u}_x\right)\left(\boldsymbol{\psi}^t \delta\mathbf{u}_s'\right) d\Gamma\, dx \tag{31}$$

$$\delta U_{xs}^c = G t \int_0^L \int_\Gamma \left(\boldsymbol{\psi}^t \mathbf{u}_s'\right)\left(\boldsymbol{\phi}_{,s}^t \delta\mathbf{u}_x\right) d\Gamma\, dx$$
$$\delta U_{xs}^d = G t \int_0^L \int_\Gamma \left(\boldsymbol{\psi}^t \mathbf{u}_s'\right)\left(\boldsymbol{\psi}^t \delta\mathbf{u}_s'\right) d\Gamma\, dx \tag{32}$$

$$\delta U_{xs}^e = \frac{G t^3}{3} \int_0^L \int_\Gamma \left(\boldsymbol{\chi}_{,s}^t \mathbf{u}_n'\right)\left(\boldsymbol{\chi}_{,s}^t \delta\mathbf{u}_n'\right) d\Gamma\, dx \tag{33}$$

being the terms $\delta U_{xs}^b, \delta U_{xs}^d$ δU_{xs}^e integrated by parts due to their dependency on the variational derivatives.

The functional gradients of (20) are identified towards the definition of the thin-walled governing equations along the beam axis as follows:

$$\frac{\partial \mathscr{V}}{\partial \mathbf{u}_x} = -\mathbf{k}_2^1 \mathbf{u}_x'' + \left(\mathbf{k}_1^4 - \mathbf{k}_1^1\right)\mathbf{u}_s' + \mathbf{k}_0^3 \mathbf{u}_x - \mathbf{p}_x = 0 \tag{34}$$
$$\frac{\partial \mathscr{V}}{\partial \mathbf{u}_s} = -\mathbf{k}_2^4 \mathbf{u}_s'' + \left(\mathbf{k}_1^2 - \mathbf{k}_1^3\right)\mathbf{u}_x' + \mathbf{k}_0^1 \mathbf{u}_s - \mathbf{p}_s = 0 \tag{35}$$
$$\frac{\partial \mathscr{V}}{\partial \mathbf{u}_n} = \mathbf{k}_4 \mathbf{u}_n'''' + \left(\mathbf{k}_2^3 + \mathbf{k}_2^2 - \mathbf{k}_2^5\right)\mathbf{u}_n'' + \mathbf{k}_0^2 \mathbf{u}_n - \mathbf{p}_n = 0 \tag{36}$$

The differential Eqs. (34) and (35) represent the membrane structural behaviour of the thin-walled beam, whereas Eq. (36) represents the flexural behaviour of the beam walls. This system of fourth order differential Eqs. (34)–(36), which corresponds to a set of equilibrium equations written in terms of displacements, can be compactly written as follows:

$$\mathbb{K}_4 \mathbf{u}'''' + \mathbb{K}_2 \mathbf{u}'' + \mathbb{K}_1 \mathbf{u}' + \mathbb{K}_0 \mathbf{u} - \mathbf{p} = 0 \quad \text{with} \quad \mathbf{p} = [\mathbf{p}_x \quad \mathbf{p}_s \quad \mathbf{p}_n]^t \tag{37}$$

where the matrices $\mathbb{K}_4, \mathbb{K}_2$ and $\mathbb{K}_0$ are symmetric, whereas the matrix $\mathbb{K}_1$ is skew-symmetric, being written as follows:

$$\mathbb{K}_4 = \begin{bmatrix} \cdot & \cdot & \cdot \\ \cdot & \cdot & \cdot \\ \cdot & \cdot & \mathbf{k}_4 \end{bmatrix} \quad \mathbb{K}_2 = \begin{bmatrix} -\mathbf{k}_2^1 & \cdot & \cdot \\ \cdot & -\mathbf{k}_2^4 & \cdot \\ \cdot & \cdot & \left(\mathbf{k}_2^3 + \mathbf{k}_2^2 - \mathbf{k}_2^5\right) \end{bmatrix}$$
$$\mathbb{K}_1 = \begin{bmatrix} \cdot & \left(\mathbf{k}_1^4 - \mathbf{k}_1^1\right) & \cdot \\ \left(\mathbf{k}_1^2 - \mathbf{k}_1^3\right) & \cdot & \cdot \\ \cdot & \cdot & \cdot \end{bmatrix} \tag{38}$$

$$\mathbb{K}_0 = \begin{bmatrix} \mathbf{k}_0^3 & \cdot & \cdot \\ \cdot & \mathbf{k}_0^1 & \cdot \\ \cdot & \cdot & \mathbf{k}_0^2 \end{bmatrix} \tag{39}$$

The submatrices $\mathbf{k}_i^j$ are presented in (A). The matrix $\mathbb{K}_4$ is singular, given the fact of having null components on the x and s degrees of freedom. The terms of the submatrix $\mathbf{k}_4$ represent the flexure of the cross-section walls, i.e., the flexure of the walls along their midline, and also the warping of the walls relatively to the corresponding thickness, which is the so-called secondary warping when compared with the global warping of the cross-section; hence, these terms depend on t^3. In general, it can be said that these components represent the *Kirchhoff* behaviour along the longitudinal direction of the beam cross-section. Matrix $\mathbb{K}_2$ is constituted by a diagonal with three matrix blocks, being each one of them non-singular. The first block of matrices $(1,1)$, submatrix $\mathbf{k}_2^1$, corresponds to the axial stiffness of the cross-section midline (where the global warping stiffness is included), and block $(2,2)$, submatrix $\mathbf{k}_2^4$, represents the transverse stiffness of the midline associated with the in-plane coordinate. The block $(3,3)$ represents two effects of the wall structural behaviour as a plate, namely: (i) the torsional behaviour, being the corresponding stiffness given by submatrix $\mathbf{k}_2^5$; and (ii) the Poisson effect associated with the longitudinal bending defined in the submatrix $\mathbf{k}_4$, which is represented by submatrices $\mathbf{k}_2^2$ and $\mathbf{k}_2^3$. Matrix $\mathbb{K}_1$ components represent two effects: (i) the Poisson effect associated with the membrane behaviour of the cross-section midline, which is given by submatrix $\mathbf{k}_1^1 = -(\mathbf{k}_1^2)^t$; and (ii) the transverse stiffness of the midline associated with the out-of-plane coordinate, given by the submatrix $\mathbf{k}_1^4 = -(\mathbf{k}_1^3)^t$. The matrix $\mathbb{K}_1$ is therefore skew-symmetric within the space of the axial and tangential coordinates of the cross-section. Matrix $\mathbb{K}_0$ is symmetric; its blocks represent: (i) the block $(1,1)$ – submatrix $\mathbf{k}_0^3$ – an out-of-plane stiffness (in the x direction) due to the shear deformation of the midline profile; (ii) the block $(2,2)$ – submatrix $\mathbf{k}_0^1$ – an in-plane stiffness (in the s direction) due to the deformation of the midline profile along its tangential direction; and (iii) the block $(3,3)$ – submatrix $\mathbf{k}_0^2$ – the transverse stiffness (in the n direction) of the cross-section, representing its structural behaviour as a frame.

The boundary terms obtained from the integration by parts of the functional (24) are defined as:

$$\left[(\delta\mathbf{u}_s)^t\left(\mathbf{k}_1^3 \mathbf{u}_x + \mathbf{k}_2^4 \mathbf{u}_s'\right)\right]_0^L \quad \text{and} \quad \left[(\delta\mathbf{u}_n)^t \mathbf{k}_2^5 \mathbf{u}_n'\right]_0^L \tag{40}$$

and those obtained from (30) are:

$$\left[(\delta\mathbf{u}_x)^t\left(\mathbf{k}_2^1 \mathbf{u}_x' + \mathbf{k}_1^1 \mathbf{u}_s\right)\right]_0^L, \quad \left[(\delta\mathbf{u}_n)^t\left(\mathbf{k}_4 \mathbf{u}_n'' - \mathbf{k}_2^2 \mathbf{u}_n''\right)\right]_0^L$$
$$\text{and} \quad \left[(\delta\mathbf{u}_n')^t\left(-\mathbf{k}_4 \mathbf{u}_n''' + \mathbf{k}_2^2 \mathbf{u}_n'\right)\right]_0^L \tag{41}$$

These boundary terms are in equilibrium with the generalised nodal forces (18) at the corresponding beam end sections, $(x = 0, L)$. Therefore, for the thin-walled membrane behaviour the following equations apply,

$$\hat{\mathbf{Q}}_x = \left(\mathbf{k}_2^1 \mathbf{u}_x' + \mathbf{k}_1^1 \mathbf{u}_s\right)_{\bar{\Gamma}} \quad \text{and} \quad \hat{\mathbf{Q}}_s = \left(\mathbf{k}_2^4 \mathbf{u}_s' + \mathbf{k}_1^3 \mathbf{u}_x\right)_{\bar{\Gamma}} \tag{42}$$

For the flexural behaviour, the expressions that correspond to the double integration by parts are written as follows,

$$\hat{\mathbf{Q}}_n = \hat{\mathbf{Q}}_{n1} + \hat{\mathbf{Q}}_{n2} \quad \text{where} \quad \hat{\mathbf{Q}}_{n1} = \left(\mathbf{k}_4 \mathbf{u}_n'' - \mathbf{k}_2^2 \mathbf{u}_n''\right)_{\bar{\Gamma}} \quad \text{and} \quad \hat{\mathbf{Q}}_{n2} = \left(\mathbf{k}_2^5 \mathbf{u}_n'\right)_{\bar{\Gamma}} \tag{43}$$

Since the formulation is based on a *Kirchhoff* hypothesis, the integration by parts has to be performed twice, which gives rise to a boundary term that produces work on the derivative of the displacement coordinate.

$$\hat{\mathbf{Q}}_n^1 = \left(-\mathbf{k}_4\,\mathbf{u}_n''' + \mathbf{k}_2^2\,\mathbf{u}_n'\right)_{\hat{\Gamma}} \tag{44}$$

3. Implementation of the model

The model presented was derived considering the approximation of the displacement field over the beam cross-section through a set of globally defined basis functions. However, it is more versatile, and computationally more efficient, to divide the cross-section into a set of rectilinear laminar elements, forming a cross-section mesh, and to consider an approximation for the displacement field defined over each thin-walled element. The assemblage of the cross-section "elements" is made by considering the compatibility between elements in terms of the middle surface displacements at the corresponding end-sections, neglecting the compatibility of the displacement field along the thin-wall thickness. The governing differential equations are established for each element, i.e., the coefficient matrices (38) and (39) are obtained for each element and for the corresponding "local" approximation functions, being the corresponding global matrices obtained through an assembly process. The approximation functions at the element level are required to have a sufficient continuity condition, in order to allow the establishment of the beam differential equations defined in (37).

Towards the model *p*-refinement ability in terms of cross-section analysis, three cross-section elements were derived by adopting different approximation functions for the axial displacement component, namely: a set of linear *Lagrange* functions – L_k element; a set of quadratic *Lagrange* functions – Q_k element; and a set of cubic *Hermite* functions – H_k element. All three elements consider for the approximation of the tangential displacement, a set of linear *Lagrange* functions, whereas for the normal displacement, a set cubic Hermitian polynomials. Hence, the elements L_k, Q_k and H_k have 8, 9 and 10 degrees of freedom respectively.

The local degrees of freedom are represented for an L_k element in Fig. (1), being the corresponding approximation functions plotted in Fig. (2). For the cross-section analysis within the beam model formulation framework, a discretization into those elements is performed considering a suitable mesh without any restrictions regarding its definition and hence not only any arbitrary polygonal geometry can be considered, but also an *h*-refinement of a rectilinear segment is possible. In order to implement the element assemblage process, it is convenient to adopt a global refererence for the cross-section. The degrees of freedom should thus be written in terms of the global coordinates, as it is represented in Fig. (3), being related to the local degrees through an appropriate transformation matrix. The coefficient matrices for each element are then computed for the local degrees-of-freedom and, in order to obtain the global coefficient matrices for the cross-section, the transformation law is applied to each coefficient matrix.

The restrictions in terms of deformability are considered through the definition of an additional set of conditions that the degrees of freedom should satisfy. In particular, in order to neglect

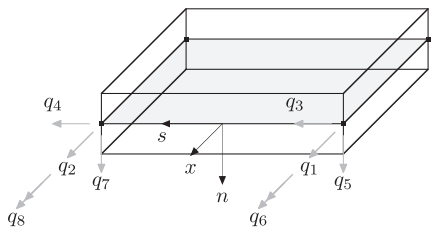

Fig. 1. Thin-walled element – degrees of freedom (local reference frame).

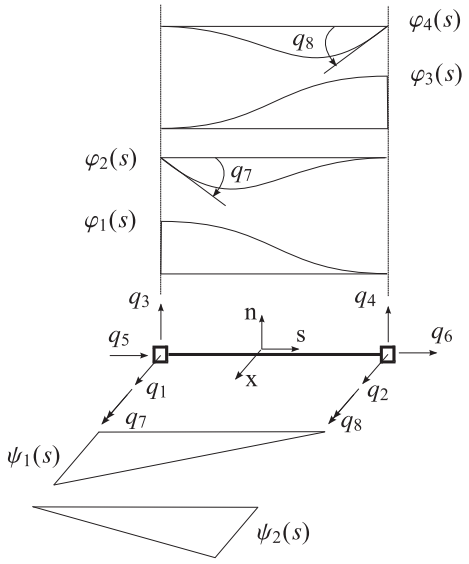

Fig. 2. Thin-walled element – L_k.

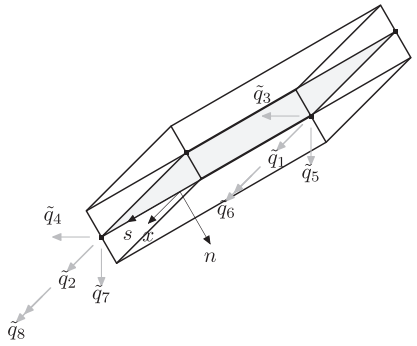

Fig. 3. Thin-walled element – degrees of freedom (global reference frame).

the tangential deformability of each cross-section wall element, the relative displacement along the element midline should be enforced to be null, i.e., the following applies for the element *i*,

$$q_4^j - q_3^j = 0 \tag{45}$$

which is written in local coordinates. For a cross-section with *n* elements, *n* similar conditions to (45) are considered, being $j = 1 \ldots n$. The set of conditions are written for the cross-section global coordinates, being written as follows,

$$\mathbf{R}_s\,\tilde{\mathbf{q}} = 0 \tag{46}$$

where the matrix $\mathbf{R}_s$ represents the set of constraints imposed and vector $\tilde{\mathbf{q}}$ stands for the global coordinates of the cross-section. Numerically, this procedure is considered by computing the null-space of the constraint matrix, $\mathbf{R}_s$, which would render a set of the remaining degrees of freedom.

In order to consider a rigid diaphragm or stiffener that prevents the cross-section distortion, a set of suitable constraints, expressed as a set of additional conditions between the transverse degrees of freedom, which are independent of the axial direction, can be implemented through the same procedure, i.e., by a matrix of the form (46). The consideration of such diaphragm in the GBT formulation of Gonçalves et al. (2009) is considered through a cross-link bracing the closed cross-section.

4. Definition of the beam deformation modes

The differential equilibrium equations presented in terms of the displacement field coordinates in Eq. (37) correspond to a coupled system due to the generality considered in the definition of the approximation functions and hence the physical interpretation of the beam structural behaviour through beam-like equations is not possible. A procedure for uncoupling the thin-walled governing equations, allowing to retrieve classic solutions and obtain higher order solutions with a physical meaning and a mathematically consistent form is a key factor for the efficient use of higher order one-dimensional models. Therefore, an uncoupling of the model must be defined towards the physical perception and understanding of the structural phenomena in a more clear way.

The uncoupling of the higher order beam formulation is based on the definition of uncoupled deformation modes, which correspond to solutions of the corresponding governing equations derived from the elasticity theory. Towards this end, a general homogeneous solution for Eq. (37) is sought in the following form:

$$u(x) = \mathbf{u}_0\, e^{\lambda x} \tag{47}$$

which being substituted into the equilibrium equations yields the following eigenvalue problem,

$$\mathbf{P}(\lambda)\,\mathbf{u}_0 = 0 \quad \text{with} \quad \mathbf{P}(\lambda) = \mathbb{K}_4\,\lambda^4 + \mathbb{K}_2\,\lambda^2 + \mathbb{K}_1\,\lambda + \mathbb{K}_0 \quad \text{and} \quad \lambda \in \mathbb{C} \tag{48}$$

where λ represents the eigenvalue variable and the $\mathbf{u}_0$ the corresponding eigenvector, being $\mathbf{P}(\lambda)$ a polynomial matrix. A deformation mode is therefore defined by an eigenvector of (48).

This approach, although considering exponential solutions, is quite different from the solution put forward by Jönsson and Andreassen (2011) for obtaining solutions to the GBT distortional modes. In fact, the authors consider an exponential solution for the higher order model differential equations and rely on solution of the corresponding quartic eigenvalue given by Eq. (48) to derive a set of orthogonal deformation modes. Both "conventional beam displacement modes" and higher order modes stem directly from the generalised eigenvectors and eigenvectors of (48) without further additional procedures.

Deformation modes associated with null eigenvalues have amplitudes corresponding to polynomial terms that represent solutions with no decay along the beam axis, being designated as fundamental modes. Deformation modes having as amplitudes exponential terms on the beam axis coordinate represent higher order modes, having thus associated a decaying pattern along the beam axis.

For the solution of the eigenvalue problem (48) the most usual way is through a linearization procedure, consisting in reducing the fourth order differential system of equations defined in (37) to a first order system of differential equations, which has associated a linear eigenvalue problem (Goheberg et al., 1982). Several linear forms can be derived, however, given the symmetric characteristics of the problem (a spectrum both symmetric to the real and imaginary axes), a linear form that preserves this structure is chosen (Tisseur, 2000; Tisseur and Meerbergen, 2001).

For the beam eigenvalue problem (48) a twelve fold null eigenvalue is obtained, having associated a geometric multiplicity of 4, which corresponds to the dimension of the nullspace of matrix $\mathbb{K}_0$. The corresponding deformation modes represent the classic solution of the problem and are defined as *fundamental deformation modes*; these modes are obtained by the associated generalized eigenvectors (Vieira, 2010), which represent a general solution for (37) of the form:

$$\mathbf{u}(x) = \left(\frac{x^k}{k!}\,\mathbf{u}_0 + \cdots, + x\,\mathbf{u}_{k-1} + \mathbf{u}_k\right) \quad \text{with} \quad \mathbf{u}_0 \neq 0 \tag{49}$$

being $\mathbf{u}_i$ with $i = 0 \ldots k$ the generalised eigenvectors associated with the null eigenvalue obtained through the solution of the corresponding Jordan chain of matrices. The generalised eigenvectors are thus obtained from the solution of the following set of equations:

$$\mathbb{K}_0\,\mathbf{u}_0 = 0 \quad \text{and} \quad \mathbb{K}_1\,\mathbf{u}_1 + \mathbb{K}_0\,\mathbf{u}_0 = 0 \quad \text{with} \quad \mathbf{u}_0, \mathbf{u}_1 \neq 0 \tag{50}$$

However, for the beam higher order formulation, the dimension of the space spanned by vectors $\mathbf{u}_0$ and $\mathbf{u}_1$ is still not equal to the algebraic multiplicity of the null eigenvalue, which implies the solution of further Jordan equations (Goheberg et al., 1982; Wilkening, 2004). Two more sets of equations were needed to achieve convergence (and hence $k = 3$), which correspond to obtain the beam generalised eigenvectors through the nullspace of an augmented companion matrix:

$$\mathbf{u}_0, \mathbf{u}_1, \mathbf{u}_2, \mathbf{u}_3 \in \mathcal{N}\mathbf{J} \tag{51}$$

being $\mathbf{u}_0, \mathbf{u}_1, \mathbf{u}_2$ and $\mathbf{u}_3$ the corresponding generalized eigenvectors and the matrix $\mathbf{J}$ defined as follows:

$$\mathbf{J} = \begin{bmatrix} \mathbb{K}_0 & \cdot & \cdot & \cdot \\ \mathbb{K}_2 & \mathbb{K}_1 & \cdot & \cdot \\ \mathbb{K}_2 & \mathbb{K}_1 & \mathbb{K}_0 & \cdot \\ \cdot & \mathbb{K}_2 & \mathbb{K}_1 & \mathbb{K}_0 \end{bmatrix} \tag{52}$$

The procedure for obtaining the deformation modes associated with the null eigenvalue (i.e. the fundamental modes) is explained with further detail in Vieira (2010) and Vieira et al. (2013).

A set of non null complex eigenvalues is also obtained from (48), being the corresponding eigenvectors defined as *higher order deformation modes*, having an associated decay length defined by the real part of the respective eigenvalue. The non null eigenvalues of (48) represent the base to derive the beam higher order deformation modes. In fact, the set of eigenvectors associated to the polinomial eigenvalue problem (48) constitutes a basis for the space of solutions of the general differential Eqs. (37), being the respective solution written as follows:

$$\mathbf{u} = \mathbf{u}_0^1\, e^{\lambda_1 x} + \cdots \mathbf{u}_0^m\, e^{\lambda_m x} \quad \text{with} \quad \mathbf{u}_0^j \in \mathbb{C}^{n_d} \text{ and } \lambda_i \in \mathbb{C} \tag{53}$$

where the following items should be regarded: (i) n_d corresponds to the problem degrees of freedom, being the matrices $\mathbb{K}_k, (n_d \times n_d)$; (ii) m represents the number of non null eigenvalues; (iii) the set $\Lambda = \{\lambda_1, \ldots, \lambda_m\}$ corresponds to the set of non null eigenvalues obtained; (iv) the elements of Λ occur in quadruplets $\{\lambda_j, \bar{\lambda}_j, -\lambda_j, -\bar{\lambda}_j\}$, being possible that some of them degenerate into pairs of reals $(\lambda_r, -\lambda_r)$; (v) the set $\{\mathbf{u}_0^1, \textit{corresponds to the problem degrees of freedom}, \mathbf{u}_0^m\}$ corresponds to the eigenvectors associated with (48); and (vi) some of the eigenvectors obtained have real components, whereas the others have complex components with a non null real part. The solution component associated with the eigenvalue $-\lambda_j$ is given by,

$$\mathbf{u}_0^j\, e^{-\lambda_j x} \quad \text{being} \quad \lambda_j = \lambda_j^{Re} + \imath\,\lambda_j^{Im} \tag{54}$$

which is rewritten according to Euler's formula as follows,

$$\hat{\mathbf{u}}_0^j\, e^{-\lambda_j^{Re} x} \quad \text{with} \quad \hat{\mathbf{u}}_0^j = \mathbf{u}_0^j \left(\cos \lambda_j^{Im} x + \imath \sin \lambda_j^{Im} x\right) \tag{55}$$

where $\imath$ stands for the imaginary number. Therefore, the real part of the eigenvalue has a precise and important physical meaning as it *measures the influence of a solution component on the overall structural behaviour through the corresponding decaying factor*. The symmetry of the eigenvalues relatively to the real axis represents the decaying effect for a position of the beam $x > 0$, negative eigenvalues, and $x < 0$, positive eigenvalues. The imaginary part provides an oscillatory amplitude along the beam axis for the solution, which represents the transverse stiffness influence on the equilibrium equations (e.g., the equations for the equilibrium of a beam on an

elastic foundation.). No pure imaginary eigenvalues are obtained. In fact, it would not make physical sense inasmuch a pure imaginary eigenvalue would imply that a periodic solution corresponding to a strained state has no energy of deformation for a beam with a length equal to the period (Synge, 1941).

The core idea driving the uncoupling procedure framework is to rewrite the initial projection of the beam displacement field (2) into a new set of coordinates, the displacement modes, that considers the uncoupling obtained in terms of the solutions components. A new basis for the displacement field approximation is then to be sought between the solutions components. By doing so, an uncoupled form of the beam differential equations with physical meaning is obtained.

However, attention needs to be paid to the fact of two different spaces and therefore different concepts of orthogonality are being herein considered: (i) the space of functions which are solutions of the homogeneous differential Eq. (37), the deformation modes; and (ii) the space of basis functions adopted for the displacement field projection on the beam cross-section, the displacement modes.

It is also convenient to remind that a major difference in relation to the more usual eigenvalue problems (standard and the generalised eigenvalue problems) is the fact that in polynomial eigenvalue problems the number of eigenvalues to obtain is superior to the problem dimension and therefore the associated eigenvectors do not form a linearly independent set of vectors (Tisseur, 2000). On the other hand, and since the eigenvectors can have complex components, an eigenvector unfolds into real and imaginary parts, which are both solutions of the beam differential equations (Braun, 1993), representing beam deformations modes.

Since an eigenvector associated with a non-null eigenvalue representing an higher order deformation mode is part of the beam differential equation solution, it contains displacement modes associated with the beam polynomial solutions (i.e. the classic solutions corresponding to the fundamental deformations modes previously defined).

From a physical perspective, it is possible to shed some light on the composition of the eigenvector associated with a non null eigenvalue. Consider the example of a thin-walled beam submitted both to a uniform torsion, which is a fundamental mode in the sense that it has a polynomial form given by the classic Saint-Venant solution, and to a non-uniform torsion by restraining the cross-section from warping, which corresponds to a decaying mode. The cross-section warping functions are the same, the theories of Umansky (1940), Vlassov (1961) and Benscoter (1954) assume that fact; it is the amplitude of the warping function along the beam axis that differ according to "how much" the warping is restrained. On the other hand, the non-uniform solution must also represent the cross-section rotation along the beam axis defined in the fundamental modes. The cross-section in-plane deformation should however be different. In fact, the cross-section could be considered rigid without compromising the results in uniform torsion, whereas for non-uniform torsion the cross-section deformation must be considered.

Therefore, an eigenvector associated with a non null eigenvector representing the non-uniform torsion of a beam is composed by a linear combination of the following fundamental modes: (i) the cross-section rotation around the beam axis; and (ii) the cross-section warping mode; and by a set of higher order modes representing the cross-section deformation in its own plane and higher order cross-section warping modes.

These facts have suggested that the fundamental modes are represented in the set of eigenvectors corresponding to the non null eigenvalues. Hence, the basis functions that correspond to the obtained fundamental modes have to be "swept" from both real and imaginary parts of the eigenvectors $\{\mathbf{u}_0^1, \ldots, \mathbf{u}_0^m\}$ defined by (53). This is performed through a Gram-Schmidt orthogonalization procedure between the set of fundamental modes and the set of higher order eigenvectors solutions. The result is a set of vectors which are orthogonal to the space spanned by the fundamental basis functions but are not necessarily orthogonal among them. Hence, a further Gram-Schmidt orthogonalization between those vectors in order to establish a basis for the higher order modes is required to finally define a set of higher order basis functions from the eigenvectors associated with the non null eigenvectors.

The result is a set of n_d linearly independent displacement modes (exactly the number of the initial set of approximation functions), which linearly combined are able to reproduce all the beam deformation modes (i.e., the corresponding solutions). Adopting these new set of basis for a change of coordinates for the beam differential Eq. (37), an uncoupled form is derived consistently, which has associated exactly the same set of eigenvalues (recall that only linear combination of basis function have been made), which proves not to modify the physical meaning of the thin-walled governing differential equations. In fact, if a different set of eigenvalues is obtained, the solution would also be different, (53). The transformation is therefore known in algebra as isospectral (Lancaster, 2005; Lancaster and Prells, 2006).

Hence, regarding the uncoupling procedure described the following criteria are established:

- uncoupled deformation modes are obtained from the eigenvalue problem associated with the model governing equations, being defined uncoupled fundamental modes through a Jordan process by the corresponding generalised eigenvectors representing classic solutions and uncoupled higher order deformation modes with a decaying pattern;
- the higher order solutions associated with eigenvalues of equal norms are equivalent, being the real part of the eigenvalue a measure for the decaying length, which allows a consistent hierarchical selection of modes;
- a set of displacement modes must be obtained from the eigendata towards the definition of an uncoupled form of the model governing equations with a physical meaning;
- the number of displacement modes obtained from fundamental modes and from higher order modes must be equal to the initial degrees of freedom for the beam displacement field approximation;
- adopting the set of displacement modes for rewriting the governing equations, the corresponding eigenvalues must be equal to the initially obtained.

5. Examples of application

5.1. cross-section analysis

The higher order beam formulation is applied to the analysis of a beam with different cross-sections, a rectangular hollow cross-section, an I shaped section, in order to illustrate the applicability of the model regarding the definition of the uncoupled deformation modes and the corresponding displacement modes. A right handed coordinate system $O(x,s,n)$ is adopted for the beam frame reference, where x corresponds to the longitudinal axis of the beam, n is the perpendicular direction to each of the cross-section walls and the coordinate s runs through the cross-section wall midline. Therefore, the (x,s) plane corresponds to the middle surface of the beam. The origin of the coordinate system is not fixed *a priori*, in fact it can be any point of the cross-section midline. The thin-walled beams analysed are made of steel with an elasticity modulus $E = 210\ \text{kN/mm}^2$.

The examples consider the discretization of the cross-section into the L_k element defined in Section 3, i.e., linear Lagrange functions for the axial and tangential displacement, x and s directions, respectively, and a set of cubic Hermitian functions for the displacements on the wall perpendicular direction, n, as represented in Fig. (3).

The cross-sections walls are admitted to be undeformable along the corresponding midline and the *Poisson* effect is neglected. Towards this end, a set of restrictions in the form of Eq. (46) is written for each cross-section, identifying the respective nullspace of the constrains matrix.

5.1.1. Hollow box-shaped cross-section

An application of the beam model cross-section analysis to a hollow box-shaped thin-walled beam is presented in this section. The cross-section has a height $h = 2000$ mm and a width $b = 1000$ mm, having all the cross-section walls a thickness of $t = 20$ mm. The cross-section is divided into four L_k elements, being the discretization, with the corresponding degrees of freedom, represented in Fig. 4. Considering the cross-section to have the walls undeformable along the corresponding midline through the following additional conditions,

$$q_5 = q_6, \quad q_8 = q_7, \quad q_9 = q_{12}, \quad q_{10} = q_{11}$$

the total number of degrees of freedom for the cross-section displacement field approximation is reduced to *twelve*, being *four* of them in the axial direction and the other *eight* along the transverse direction.

The computation of the associated eigenvalue problem renders *twelve* null eigenvalues and *twenty-eight* non null eigenvalues, which occur in *five* sets of quadruplets complex values and *four* pairs of reals.

Due to the singularity of the problem, recall that this polynomial eigenvalue is not full ranked given the fact that the matrix $\mathbb{K}_4$ being singular, *eight* infinity solutions were obtained. All summed up, a total of *forty* eigenvalues were obtained plus *eight* singularities, which correspond to four times the problem degrees of freedom, *twelve*, as it should, since this is a quartic eigenvalue problem.

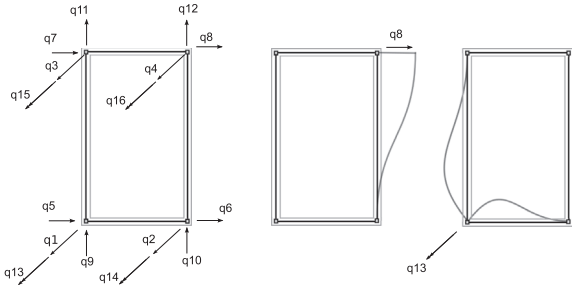

Fig. 4. Box section discretization – 4 elements.

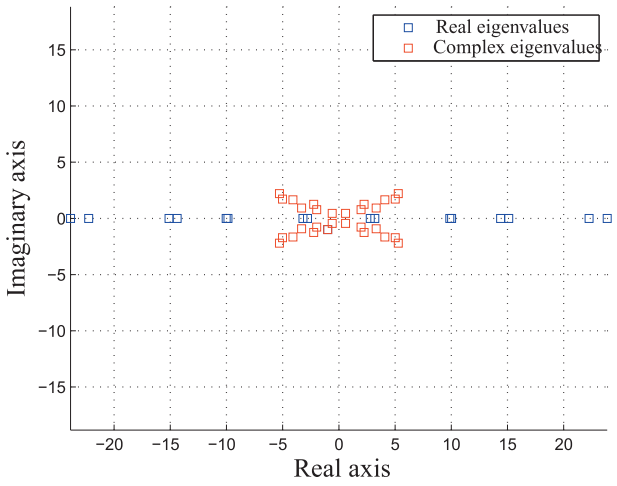

Fig. 6. Box Beam, eigenvalues.

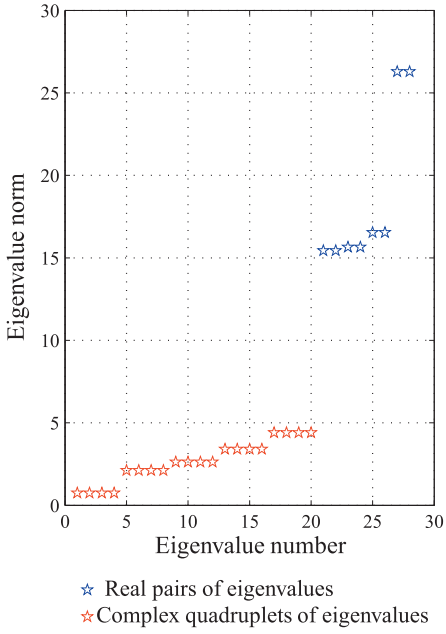

Fig. 7. Box Beam, eigenvalue norms.

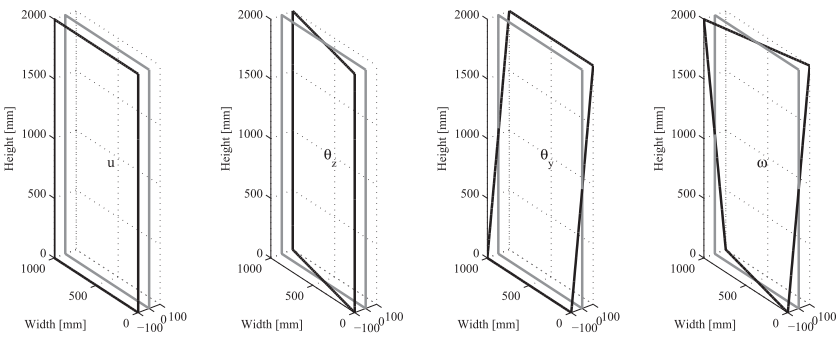

Fig. 5. Box Beam warping modes.

The *twelve* null eigenvalue imply the solution of a Jordan chain in order to identify the deformation modes associated with the classic elasticity solutions. The generalised eigenvectors obtained from (51) correspond to the beam Saint Venant solution, representing the beam extension, flexural and torsional behaviour. By adopting the procedure describe in Vieira et al. (2013), seven displacement modes are identified. The cross-section first order warping represented in Fig. 5 is obtained from the generalised eigenvector corresponding to the beam uniform torsion.

The non null eigenvalues are represented in Fig. 6 where it can be observed their symmetry relatively to both, the imaginary and the real axes. The corresponding eigenvalue norms are plotted in Fig. 7, where it can be observed that the last eigenvalue has a significant higher norm when compared with the first ones, which corresponds to a bigger decaying of the displacement field along the beam axis and, therefore, to a less importance of the associated mode in the overall structural behaviour.

The deformation modes associated with the non null eigenvalues allowed to obtain 5 basis functions for the displacement field representing the higher order modes of the cross-section, which are represented in Fig. 8, modes β_1 to β_5. Recall that 7 basis functions were identified from the generalised eigenvectors representing the classic modes and therefore the set of basis functions is complete with a total number of 12 = 7 + 5, which corresponds to the initial number of approximation functions. The displacement mode β_1 represented in Fig. 8 correspond to the cross-section distortion, whereas the mode β_2 represents a symmetric transverse flexure of the cross-section. The displacement modes β_3 to β_5 represent "higher" cross-section transverse flexural modes. Considering a change of coordinates by adopting the new set of orthogonal basis functions, the polynomial eigenvalue was solved yielding the following set of eigenvalues:

$$\pm 0.5865 \pm 0.4624i, \quad \pm 1.9039 \pm 0.9204i, \quad \pm 2.2139 \pm 1.4059i, \quad \pm 3.1608 \pm 1.2662i, \quad \pm 3.9462 \pm 1.9603i, \quad \pm 15.4381, \quad \pm 15.6482, \quad \pm 26.2838 \tag{56}$$

which correspond to the values initially obtained; it is therefore verified that the transformation is isospectral and thus the system of governing equation represents the structural behaviour of the thin-walled beam.

Table 1
Eigenvalue modal decomposition.

Deformation modes	Displacement modes combination	Eigenvalues
Non-uniform torsion	$\omega + \theta + \beta_1 + \beta_5$	$\pm 0.5865 \pm 0.4624i$ $\pm 3.9462 \pm 1.9603i$ ± 15.4381 ± 26.2838
Transverse flexure local mode	β_2	$\pm 1.9039 \pm 0.9204i$
Bending in (x,z) plane	$v + \theta_z + \beta_3$	$\pm 2.2139 \pm 1.4059i$ ± 15.6482
Bending in (x,y) plane	$w + \theta_y + \beta_4$	$\pm 3.1608 \pm 1.2662i$ ± 16.5391

From the process of decomposing the deformation modes through processes of orthogonalization (Gram-Schimdt operation and Singular Value Decompositions) it is possible to obtain a matrix that correlates the displacement modes associated to a deformation mode and hence a specific eigenvalue. This spectral decomposition/analysis proves to be relevant since it enhances the understanding of the modes obtained. In fact the 28 non null eigenvalues can be obtained separately by computing the corresponding polynomial eigenvalue problem written for a set of combination of displacement modes. In the Table 1, the sets of orthogonal displacement modes and the corresponding eigenvalues obtained are indicated, being identified 4 linear combinations of orthogonal displacement modes to obtain the initial 28 eigenvalues. The hierarchical nature of the model allows to neglect higher modes in a consistent form; e.g., if the displacement mode β_5 was neglected in the definition of the non-uniform torsion, the corresponding eigenvector would be $\pm 0.5871 \pm 0.4636i$, which represent an accurate approximation of the corresponding value in table associated with the non-uniform torsion deformation mode.

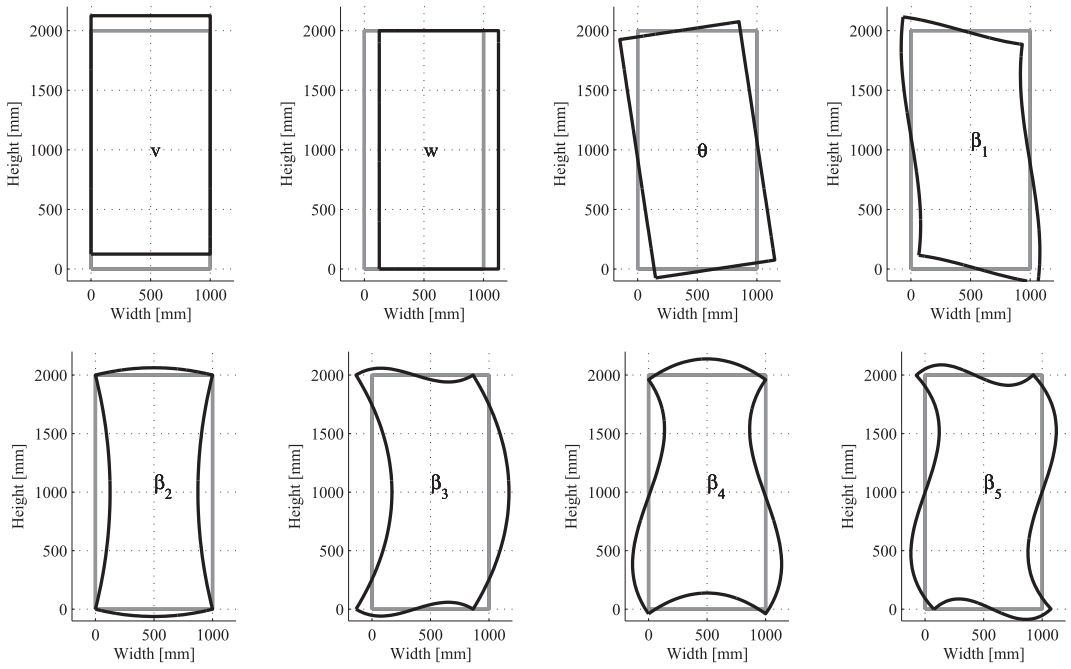

Fig. 8. Box Beam higher order modes.

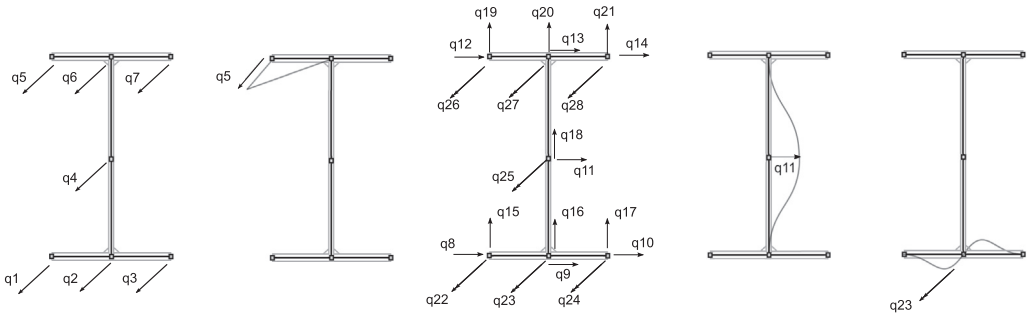

Fig. 9. I section discretization.

5.1.2. I section

A steel plated beam having a web with dimensions $1200 \times 20\ \text{mm}^2$ and equal flanges of dimensions $600 \times 50\ \text{mm}^2$ is considered. The cross-section is divided into 6 elements of the type L_k, being the corresponding degrees of freedom represented in Fig. 9.

The total number of degrees of freedom of this cross-section is 28; however, restricting the tangential deformation of the walls, see Eq. (45), through the introduction of the following additional conditions,

$$q_8 = q_9 = q_{10}; \quad q_{12} = q_{13} = q_{14}; \quad q_{16} = q_{18} = q_{20}.$$

this number is reduced to 22. The quartic eigenvalue problems yields $88 = 4 \times 22$. Computing the corresponding eigenvalue problem according to (48), the following results are obtained: (i) 14 infinite eigenvalues; (ii) 12 null eigenvalues with an algebraic multiplicity of *twelve*, which corresponds to the non decaying solution of the problem (polynomial), being capable of representing the Saint-Venant solution through the set of the associated generalised eigenvectors; and (iii) 62 non null eigenvalues, occurring in pairs of real symmetric values and in quadruplets of symmetric and conjugate complex values (corresponding to six quadruplets and nineteen pairs of eigenvalues), which represent the higher order solution with a decaying pattern along the beam axis.

The set of the generalised eigenvectors allows the definition of orthogonal displacement modes, corresponding to the classic solutions of extension, flexure and warping and a shear warping mode. The higher order modes were obtained from the eigenvectors of the quartic eigenvalue problem associated with non null eigenvalues considering the process described in Section 4. A set of out of plane warping and in-plane distortional modes were obtained. The classic modes are represented in Fig. 10. The higher order warping modes of the cross-section ω_1, ω_2, and ω_3 (Fig. 11) represent shear related modes that can be adopted to refine the analysis of the cross-section regarding its out-of-plane structural

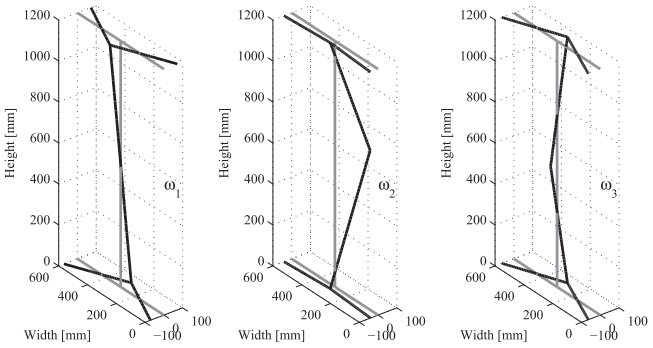

Fig. 11. I section out-of-plane higher order modes.

behaviour. The transverse distortion displacement patterns of higher order modes (modes: β_1 to β_{12};) are represented hierarchically, taking into account the corresponding eigenvalue, in Fig. 12.

5.2. Other cross-sections

In order to illustrate the versatility of the proposed model to deal with cross-section of arbitrary geometry three cross-section are considered: (i) a two cell bridge box girder with side cantilevers made of concrete (C30/37 class); and two steel sections previously considered by GBT formulations, (ii) a channel with hollow flanges considered by Gonçalves et al. (2009) and an I section shaped cross section with unequal flanges and with end stiffeners analysed in Dinis et al. (2006).

The element considered in the approximation for the three cross-section considers both linear functions for the axial and tangential component of the displacement and Hermite functions for the normal displacements. The Poisson coefficient was neglected as well as the transverse extension along the wall midline. The

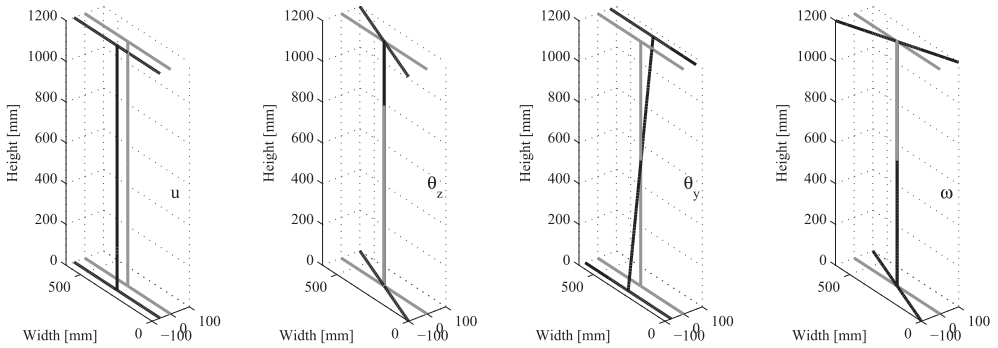

Fig. 10. I section out-of-plane classic modes.

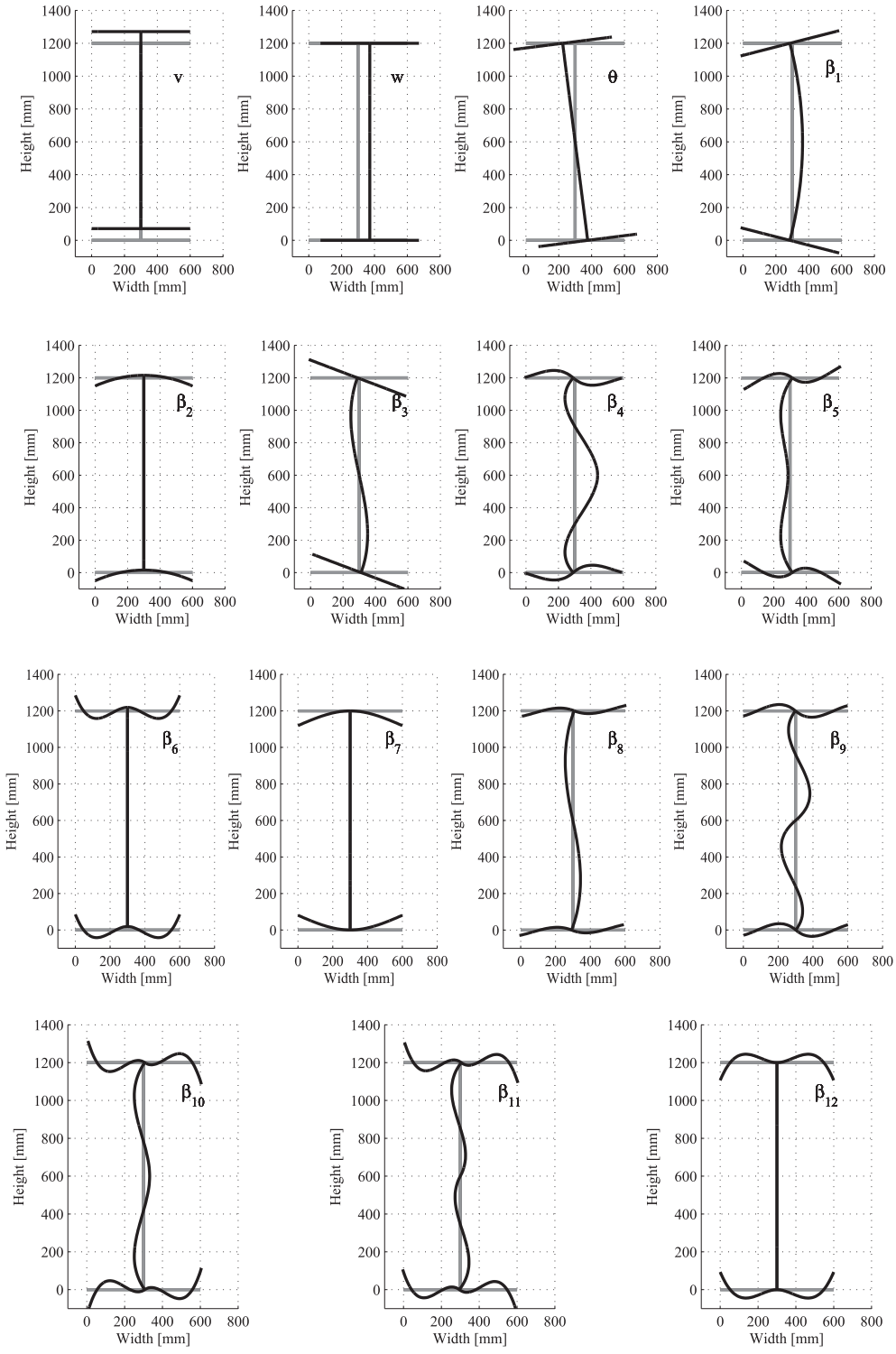

Fig. 12. I section in-plane higher order modes.

cross-section discretizations together with the corresponding dimensions are represented in Fig. 13.

The deformation modes were obtained from the solution of the non-linear eigenvalue problem, being the classic modes associated with the twelve fold null eigenvalue which required the computation of the corresponding Jordan chains. From the orthogonalization procedure, a set of orthogonal displacement modes was obtained that when adopted for a change of basis for the corresponding beam equations allows an uncoupling of the beam equations and yields the same eigenvalue set (i.e. it represents an isospectral transformation).

For the box girder and for the channel cross-sections both warping and in-plane higher order modes are presented, whereas for the I section only the in-plane modes are represented. The classic deformation modes obtained from the generalised eigenvectors correspond to the axial extension, flexure around both axes, uniform torsion and rigid body motion, being however only represented the rotation of torsion defined by θ.

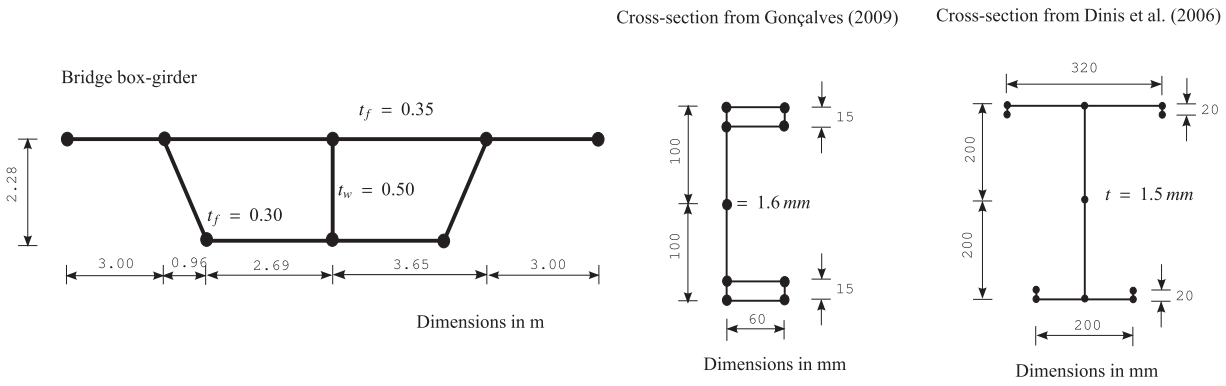

Fig. 13. Cross-sections.

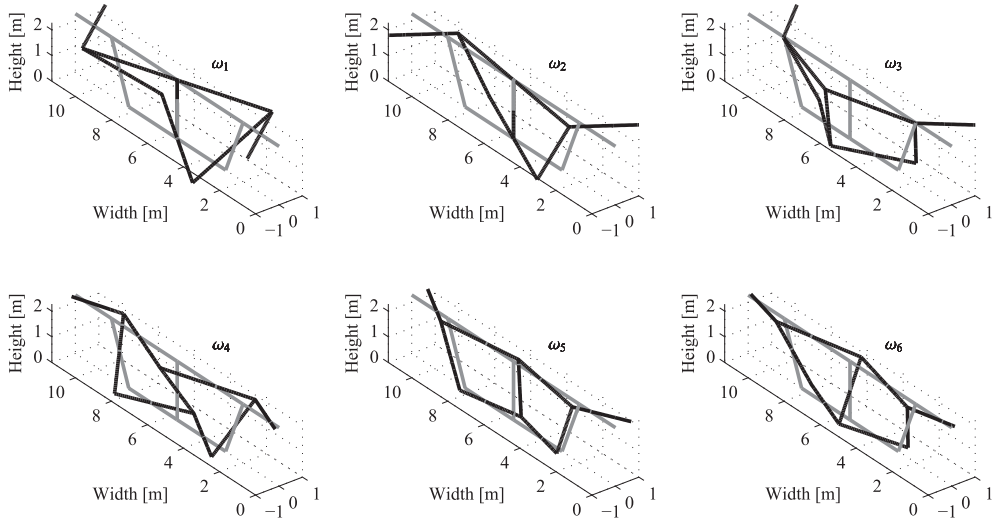

Fig. 14. Box girder out-of-plane higher order modes, ω_1 to ω_6.

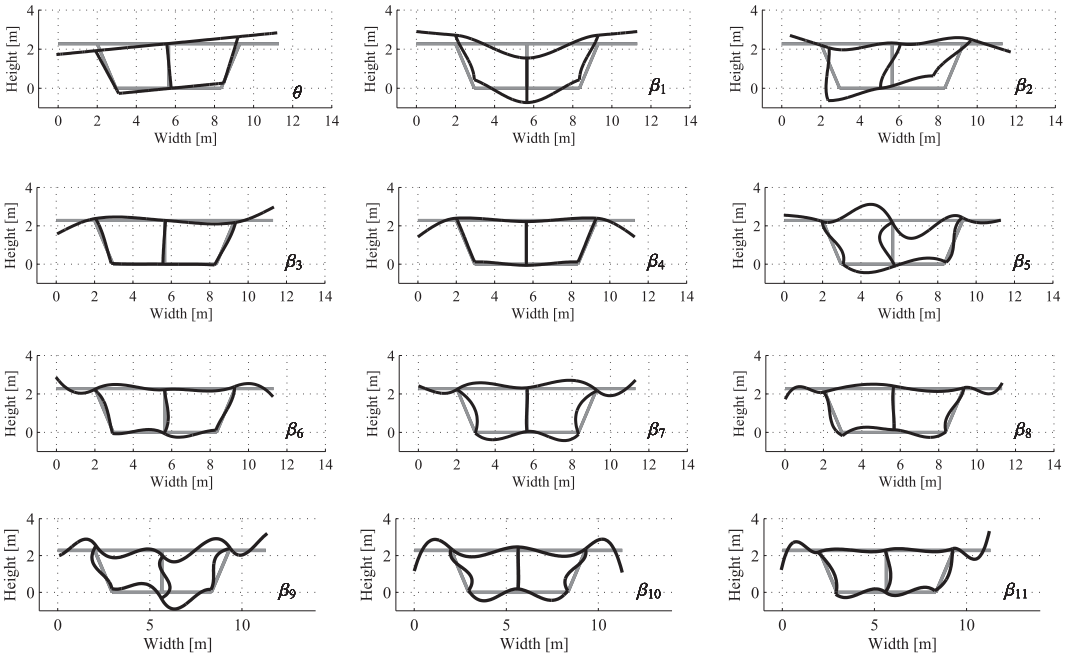

Fig. 15. Box girder in-plane higher order modes.

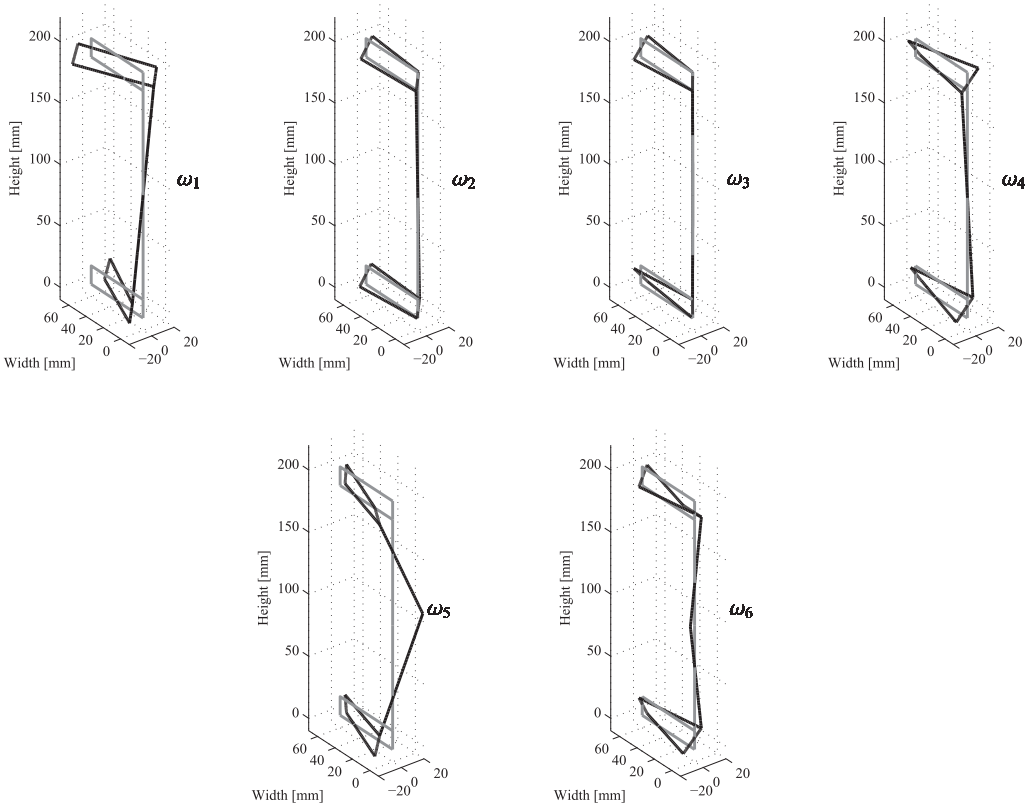

Fig. 16. Channel section warping modes.

The 6 higher order warping modes for the box-girder are represented in Fig. 14, ω_1 to ω_6 . The warping mode ω_1 represents the warping associated with the non-uniform torsion. The in-plane displacement modes are represented in Fig. 15; the rotation associated with torsion represented by θ and in-plane higher order displacement modes by β_1 to β_{11}; mode β_1 is associated with flexural behaviour representing a transverse flexure of the cross-section cells, representing the modes β_3 and β_4 local flexure modes of the overhang flanges; the in-plane transverse mode β_2 is associated with the girder torsional behaviour.

The warping modes for the channel with hollow flanges are represented in Figs. 16; a total of 6 warping modes were obtained, where ω_1 represents the warping associated with the non-unform torsion of the cross-section; ω_2 and ω_3 represent the local out-of-plane flexure of each hollow flange (symmetric and skew-symmetric modes), being the warping of both hollow flanges represented in through $\omega_4; \omega_5$ and ω_6 represent shear modes.

The rotation associated with torsion θ and the higher order in-plane modes (β_1 to β_{11}) are represented in Fig. 17. The two first higher order modes correspond to web flexural modes (symmetric and skew-symmetric); the mode β_1 is associated with the flexural behaviour around the cross-section weak axis, whereas the mode β_2 represents the distortional associated with the non-uniform torsion. Higher order modes of β_1 and β_2 involve the transverse flexure of the hollow flange as well, being defined by β_4 and β_3, respectively. The modes obtained from the GBT formulation, applied to the same cross-section, are represented in Fig. 18.

The in-plane displacement modes for the I section with unequal flanges are represented in Fig. 19. The first two higher order modes β_1 and β_2 represent distortional modes that due to the unequal width of the flanges represent uneven web flexure modes. Distortional modes involving essentially the flexure of flanges, β_6 and β_8, correspond to different decay lengths. The in-plane deformation modes obtained from GBT by Dinis et al. (2006) are represented in Fig. 21.

Some differences can be observed between the modes obtained from the GBT and those obtained through the developed model. In the GBT solution, and for the channel hollow cross-section, the torsional mode is not captured as a result of the procedure adopted for the definition of modes for this type of cross-section, which is acknowledge in Gonçalves et al. (2009). On the other hand, the modes obtained from the higher order formulation allow to capture the uniform torsion through modes ω_1 and θ, directly from the generalised eigenvectors associated with the null eigenvalue, and also the non-uniform torsion through modes $\omega_1, \theta, \beta_2$ and β_3, which are obtained applying the uncoupling procedure described in Section 4; i.e., through the eigenvectors of the non-linear eigenvalue problem associated with the beam governing equations. It should also be mentioned that by using the modes depicted in Figs. 16 and 17 for rewriting the beam differential equations, the eigenvalues obtained from the associated eigenvalue problem are exactly the same as those initially obtained. Furthermore, a spectral decomposition of modes allows to neglect higher order modes in a consistent form and without significative loss of accuracy by limiting the deviation of the corresponding eigenvalues, as exemplified in Section 5.1.1.

Modes β_1 and β_2, which correspond to the first higher order modes, are not represented explicitly in GBT. In fact, these distortional modes β_1 and β_2, which are associated with a higher decay length (and thus more relevant in the overall structural behaviour of the thin-walled beam) and represent a web flexural mode without local flexure of both hollow flanges, are not captured by GBT; conversely, the solution obtained from GBT present modes 5 and 6, which involve web flexure and simultaneously local flexure of the hollow flanges. The GBT distortional modes associated with the web flexure are captured through modes ranked 15 and 16,

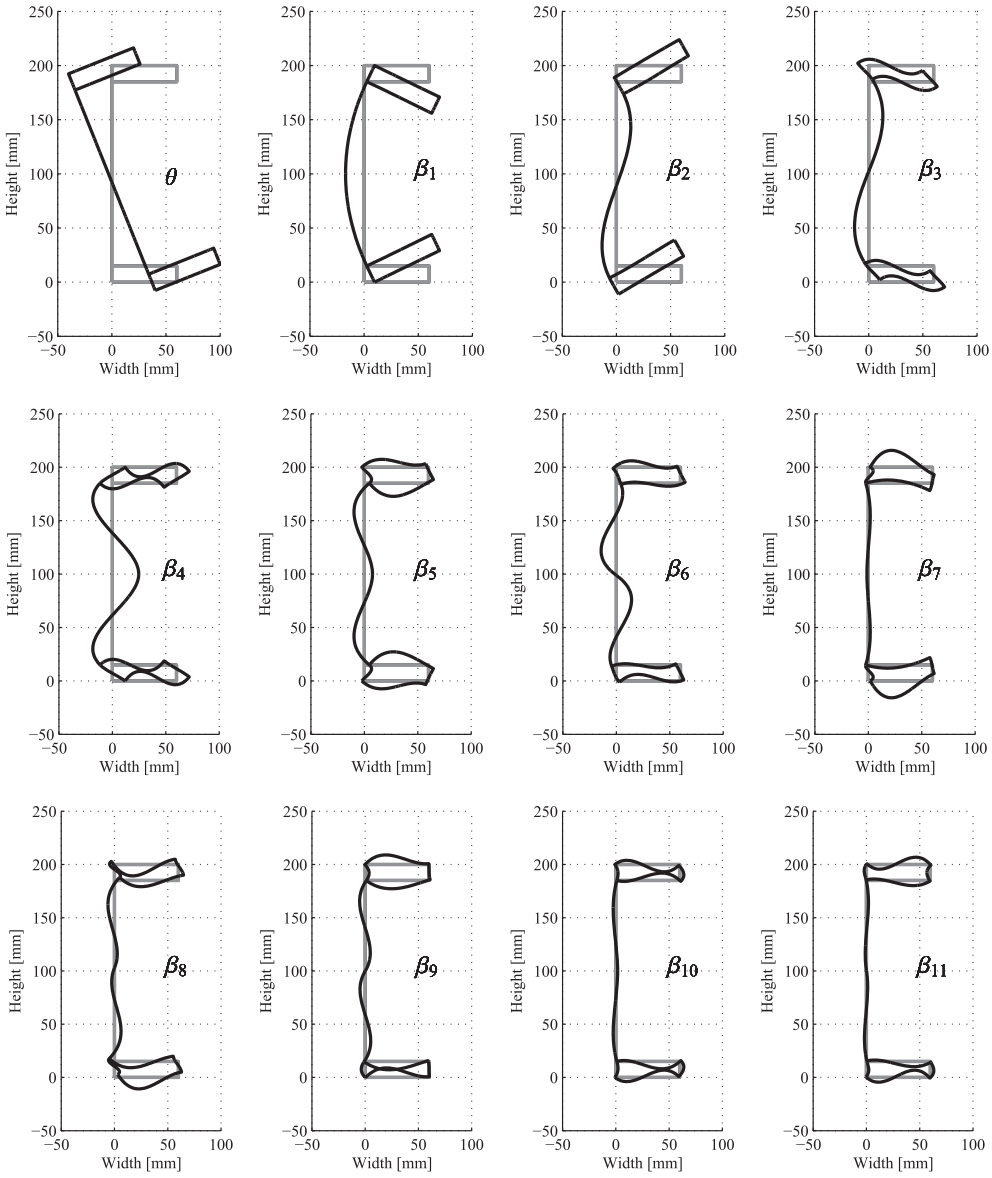

Fig. 17. Channel section in-plane higher order modes.

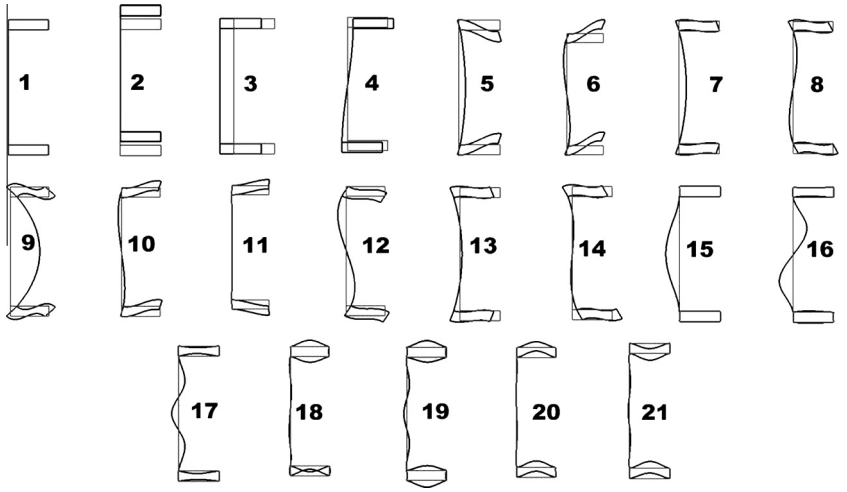

Fig. 18. Channel section in-plane deformation modes from GBT by Gonçalves et al. (2009).

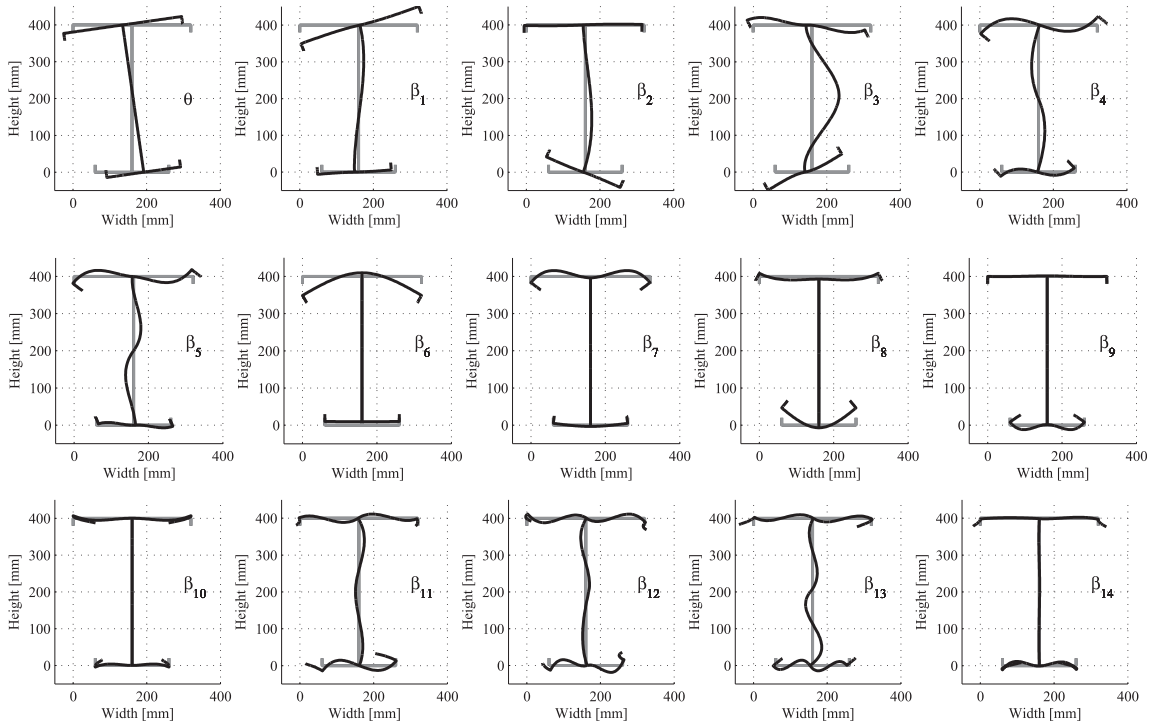

Fig. 19. I section with unequal flanges in-plane higher order modes.

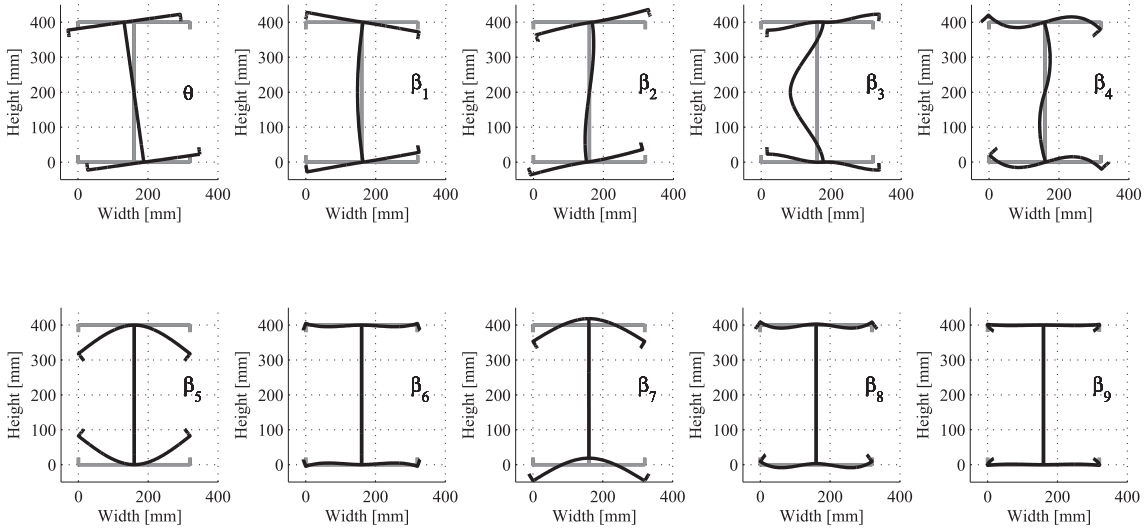

Fig. 20. I section with equal flanges in-plane higher order modes.

in which the hollow flange seems to fully restrain the web from flexure.

For the I section with unequal flanges, the GBT formulation presents distortional modes 5 and 6, whereas the higher order model defines modes β_1 and β_2 as the first higher order modes. If, on one hand, mode 6 and β_2 present a similar shape, involving the lower flange rotation, on the other hand, mode β_1 (corresponding to the upper flange) is not represented in GBT modes; instead, the mode 5 is presented, where both flanges rotate. However, modes 7 and 8, which represent the upper an lower flexure flexure are presented separately similarly to modes β_6 and β_8.

To compare the influence of unequal flanges, a similar I section but with flanges with equal widths (320 mm) was analysed, being the corresponding modes depicted in Fig. 20. The distortional mode β_1 represent an even web flexure mode, being the higher modes associated with the flexure of the flanges grouped in symmetric and skew-symmetric parts, β_5 and β_7, respectively.

5.3. Beam longitudinal analysis

The analysis of a cantilever beam through the thin-walled higher order model developed is presented in order to prove the applicability of the one-dimensional model to the three-dimensional analysis of thin-walled structures. The results obtained were compared with finite element models implemented in Abaqus (2006), in order to check the validity/accuracy of the proposed model.

Consider the I shaped cross-section, which cross-section analysis was already performed in Section 5.1.2. The bottom and upper

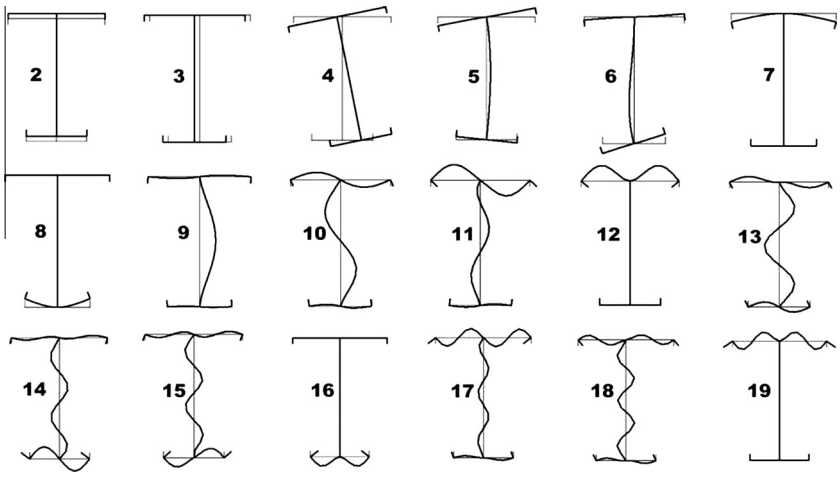

Fig. 21. I section in-plane deformation modes from GBT by Dinis et al. (2006).

flange are 600 mm width plates with a thickness of 20 mm. The beam web is a plate with 1200 × 10 mm. The cross-section is made up of steel with an elasticity modulus of $E = 210$ GPa. A cantilever beam 5000 mm long subjected to an eccentric tip load of 100 kN is analysed. The basis functions for the approximation of the displacement field over the cross-section correspond to the orthogonal set of functions obtained in Section 5.1.2.

For the solution of the beam differential equations written in the new orthogonal coordinates the finite element method was adopted considering each mode amplitude interpolated by the *Hermite* functions and a mesh of 10 equally spaced finite elements. The full restraint condition at one of the boundaries is considered by imposing that the amplitudes of all modes should cancel at this support. Notice that since this is a shear deformable theory there is no *a priori* relation between the modes coordinates and the corresponding derivatives. Therefore, the full fixed restraint only prevents the modes and not their derivatives. The cross-section is prevented to rotate but the derivative of the corresponding transverse displacement at the support is free. The deformed configuration obtained from the finite element developed is represented in

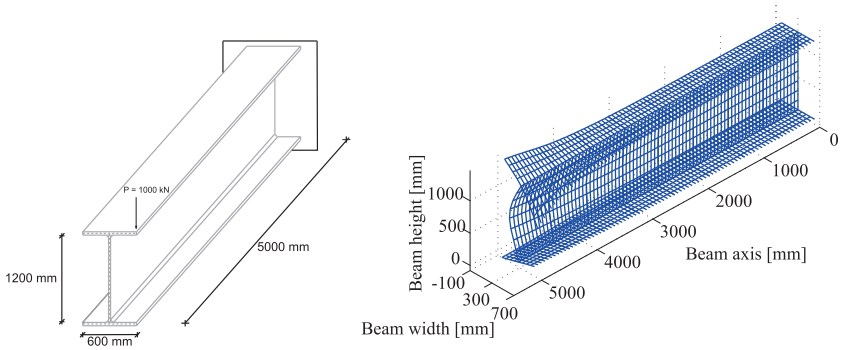

Fig. 22. Cantilever beam and corresponding deformed configuration due to an eccentric tip load.

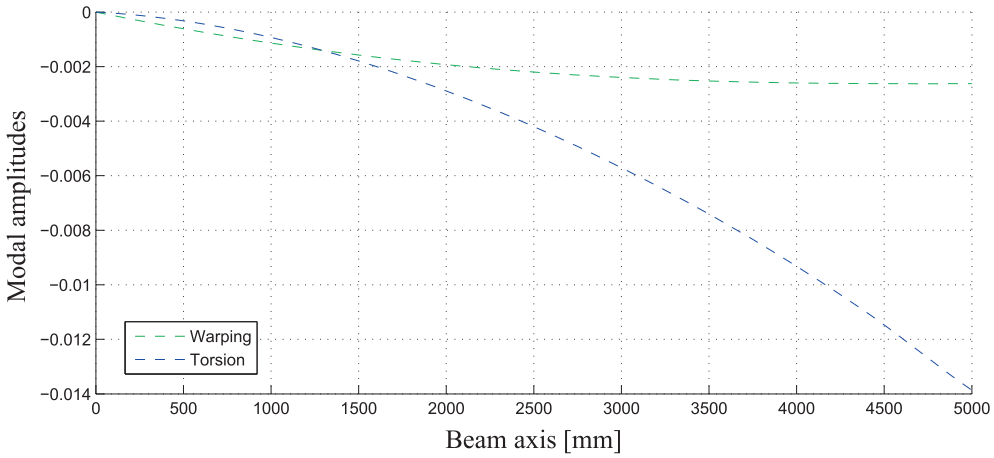

Fig. 23. Warping and torsion amplitudes.

Fig. 22. Towards the plotting of the thin-walled deformed configuration, the displacement field obtained from the one-dimensional higher order model was computed in a "mesh" (sampling points) defined over the beam cross-section profile and lengthwise along the beam axis. Firstly, the coordinates for each of the basis functions were obtained from the finite element solution and thereafter the displacements along a mesh of the profile were computed. Lengthwise, these displacements were evaluated using the interpolation functions of the longitudinal mesh. Notice that these are only sampling meshes for the displacement field and not the discretizations adopted for the cross-section analysis or the finite element solution, i.e. the deformed was obtained by a one-dimensional model.

The distribution along the beam axis of the cross-section modal amplitudes due to the warping and torsion are given in Fig. 23. The longitudinal distribution of the amplitudes for the most significative higher order modes, distortional mode and flange flexural mode represented in Fig. 12, β_1 and β_2 respectively, are plotted in Fig. 24, where for comparison purposes β_7 and β_8 are also represented. For comparison, each modal distribution was normalized relatively to the maximum value of the corresponding mode. It is therefore clear that the mode corresponding to the flange flexure, Fig. 12: β_2, has a more rapid decay than the distortional mode, β_1.

The beam stress field is computed taking in account the modal amplitudes distributions obtained together with the corresponding deformation modes. The stress components are evaluated in a mesh of sampling points, which consists in 10 equally spaced intervals per finite element, lengthwise, and 4 equally spaced intervals per cross-section element. The stress field is presented regarding the components relative to the thin-wall membrane behaviour, which are identified by $(^M)$, e.g., σ^M_{xx}, and the components relative to the thin-wall flexural behaviour that are represented through $(^F)$, e.g., σ^F_{ss}. The membrane axial stresses are plotted in Fig. 25 for the cross-section upper flange having maximums at the full fixed support and decaying along the beam axis towards its free end. On the other hand, the flexural behaviour

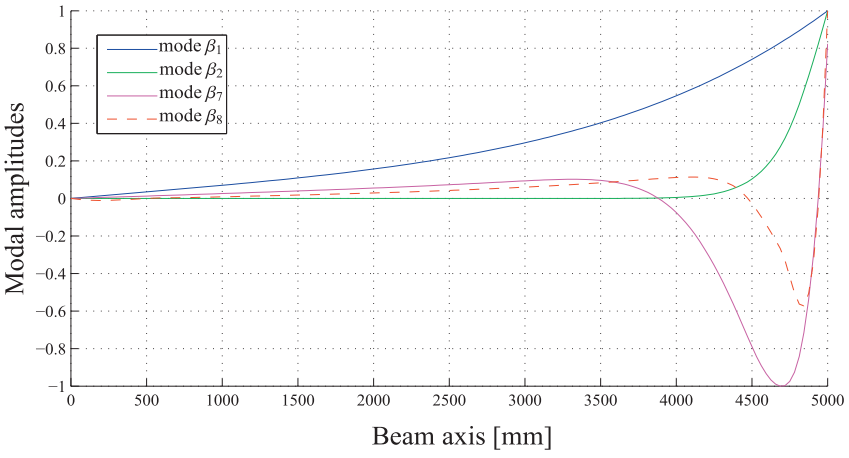

Fig. 24. Higher order modes amplitudes.

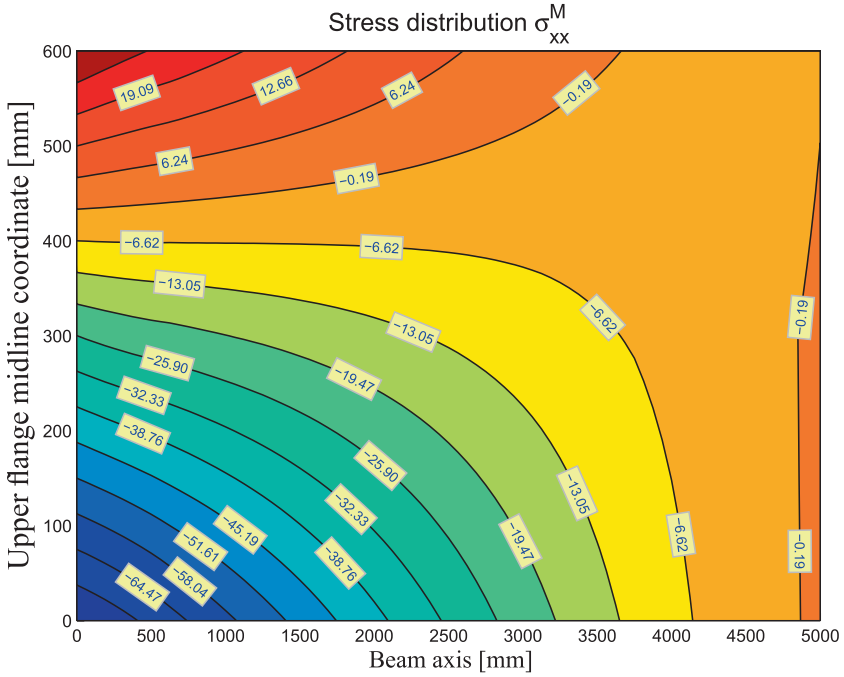

Fig. 25. Stress colour map – σ^M_{xx}, upper flange.

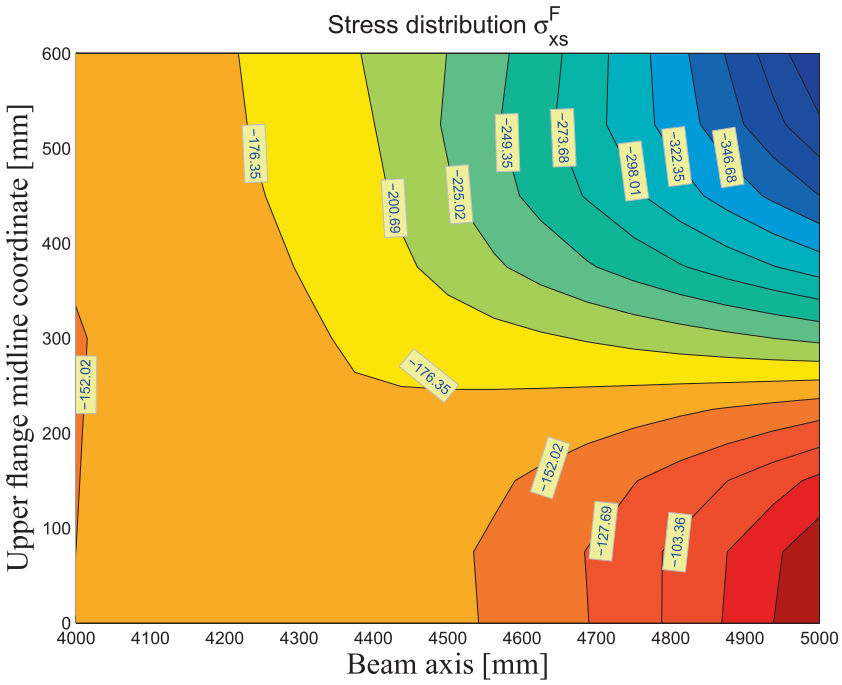

Fig. 26. Stress colour map – σ^F_{xs}, upper flange.

has a strong local effect at the load application region, being irrelevant at the beam support. In fact, the dominant structural behaviour at the edge section is due to the shell behaviour of both flanges and web, which are submitted to the concentrated load. The high stresses developed, associated with the flexure of these plates, are due to the fact that no diaphragm/stiffener is considered at the section where the load is applied. The stresses due to the flexural behaviour of the beam web are represented by the torsional component in Fig. 26.

Since the flexural behaviour at the section where the load is applied would introduce higher stresses, which the steel section would not be able to resist, a section diaphragm/stiffener made through a plate welded at the beam end section should be adopted. This plate is considered to be sufficiently stiff in order to prevent the distortional modes of the end section where the load is applied. The structural behaviour of this end section would be significantly modified, since the shell behaviour of the flange and web is prevented by the diaphragm. Therefore, the high flexural stresses observed previously should now diminish and hence the local effect becomes somewhat irrelevant when compared with the global structural behaviour, an example is available in Vieira (2010).

A comparison between the thin walled beam model developed and a shell finite element model implemented in Abaqus (2006) is presented. The thin-walled beam model considers: (i) a cross-section discretization dividing the beam web and both flanges into 4 L_k equally spaced elements, rendering a mesh with a total of 12 elements for the cross-section; the transverse deformability along the plate midline was considered as well as the Poisson effect, and thus the cross-section has a total of 52 degrees of freedom; and (ii) in terms of longitudinal analysis, a mesh with 20 finite elements, 4 in the first half of the beam length (next to the support) and 16 in the second half of the length (next to the end section).

On the other hand, the model implemented in Abaqus (2006) is based on a mesh of shell elements, which are designated by S4

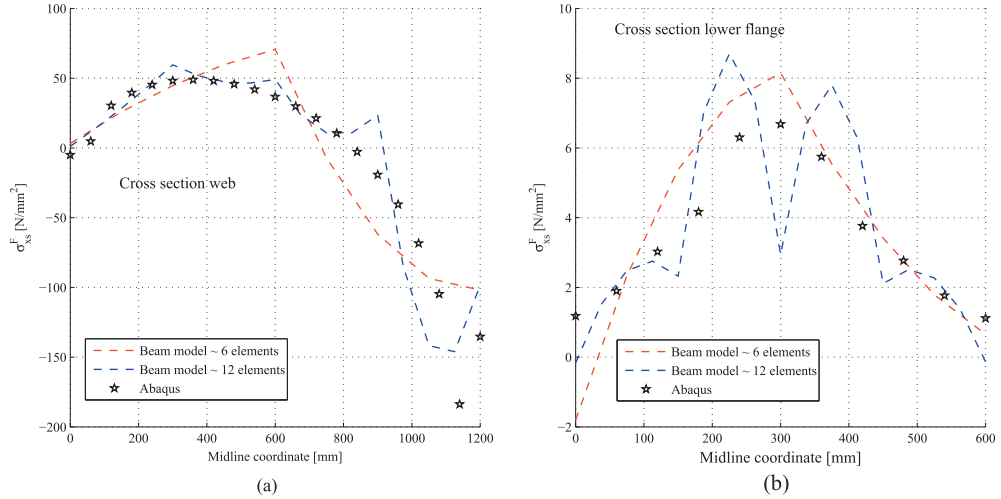

Fig. 27. Transverse torsional stresses – web and lower flange.

from the (Abaqus, 2006) library. The discretization adopted considers 40 elements per section, 10 for each flange and 20 for the web, being used 100 elements along the beam. The boundary condition corresponding to the built end section allows the corresponding nodes rotational degrees of freedom, restraining appropriate displacements. The results were compared in terms of stresses both along the beam axis and on the beam end cross-section without the stiffener. The longitudinal distribution of the thin-walled middle surface stresses, membrane behaviour, along the beam axis were in a good correlation with the results obtained from the shell model. The transverse distributions of stresses along the cross-section midline profile are represented for the end sections in Figs. 27–29. The transverse stress distributions were obtained from the cross-section discretization into 12 elements and also considering a less refined approximation of 6 elements. The transverse torsional stresses are represented along the web surface, Fig. 27(a), and along the cross-section lower and upper flange flange, Figs. 27(b) and 28(b), respectively. The transverse flexural stress for the lower and upper flange are represented in Figs. 28(a) and 29(a), and for the web in Fig. 29(b). The comparison between the formulation herein developed, identified as "Beam model", and the (Abaqus, 2006) model are fairly satisfactory, in particular taking in account that the formulation presented corresponds to a beam model with only 88 degrees of freedom, whereas in Abaqus (2006) a three-dimensional shell model with a mesh of 24846 elements was adopted.

The thin-walled beam model is applied to the analysis of a cantilever with 1000 mm length and with the channel cross-section with hollow flanges previously presented, submitted to a tip load of 5 kN as represented in Fig. 30. All the displacement modes represented in Fig. 17 were considered for the analysis, being a solution for the corresponding model differential governing equations obtained within the framework of a finite element analysis; a finite element model with 100 elements along the length is considered in the analysis. Simultaneously, and towards a validation of the higher order beam model, a shell finite element model was analysed in Abaqus (2006). For the discretization of the shell model, it was considered the structure discretized into S4 elements from the (Abaqus, 2006) library as follows: transversally, the web is divided into 4 elements and each hollow flange into 8 elements associated with a lengthwise mesh of 100 elements; the built end section is considered by preventing nodal displacements but allowing the corresponding rotational degrees of freedom.

The results in terms of membrane stresses are represented in Fig. 31 and 32 for the warping stresses (σ_{xx}^{M}) in the upper and lower flange respectively; the shear components (σ_{xs}^{M}) are represented in

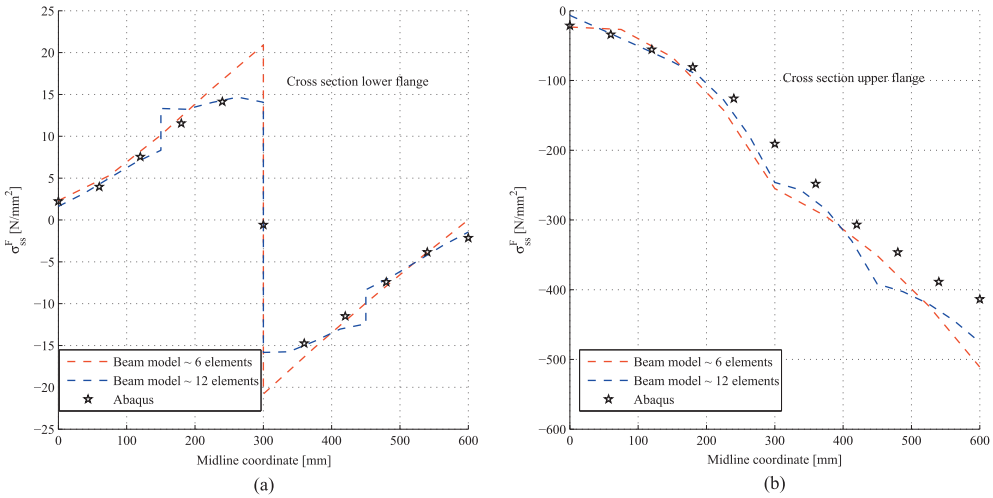

Fig. 28. Transverse flexural stress – lower and upper flange.

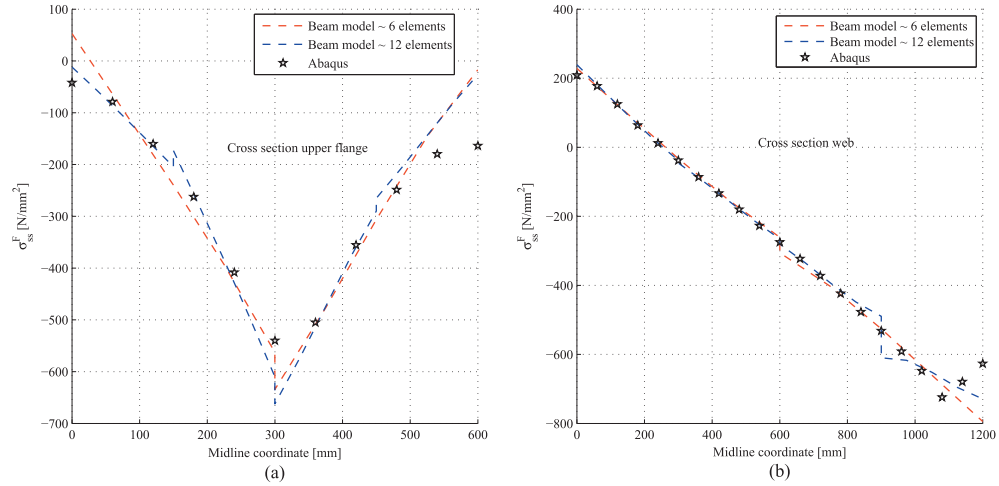

Fig. 29. Transverse flexural stress – upper flange and web.

Fig. 33. The stresses are related to the nodes defined in Fig. 30, being compared the values obtained from the developed higher order beam model and the corresponding values obtained from the shell finite element model. An interesting effect associated with the hollow flange warping is identified near the free edge.

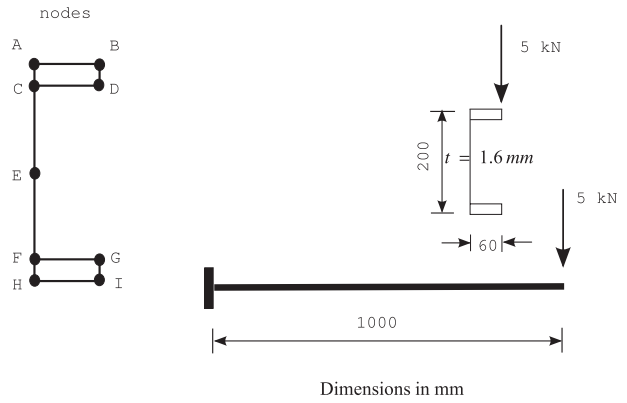

Fig. 30. Cantilever beam – channel hollow section.

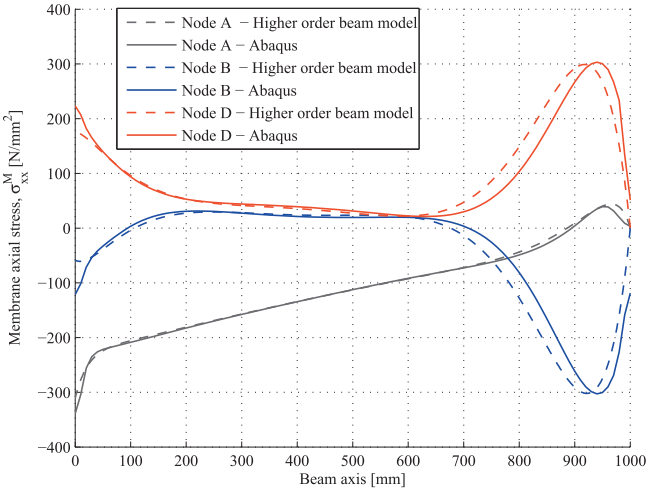

Fig. 31. Longitudinal distribution of σ^M_{xx} (upper hollow flange).

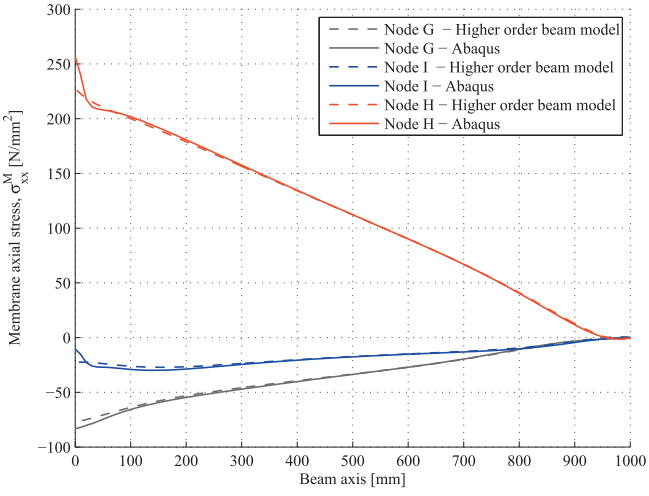

Fig. 32. Longitudinal distribution of σ^M_{xx} (lower hollow flange).

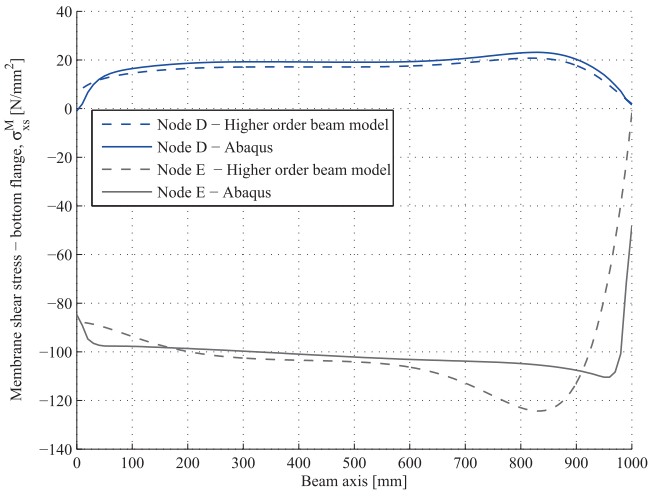

Fig. 33. Longitudinal distribution of σ^M_{xs} .

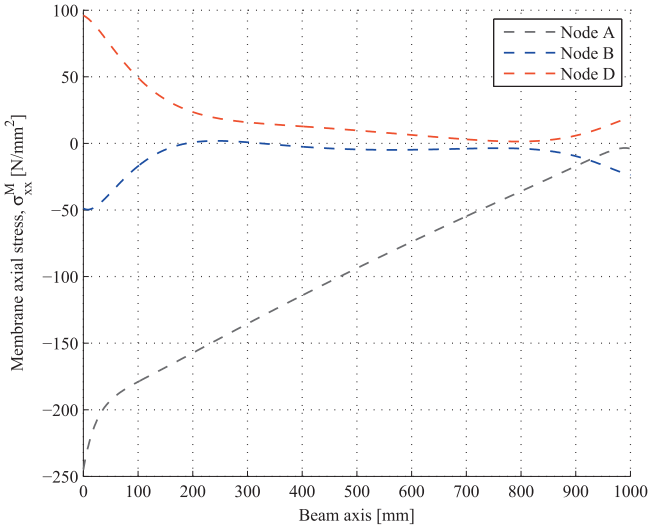

Fig. 34. Longitudinal distribution of σ^M_{xx} (with end stiffener).

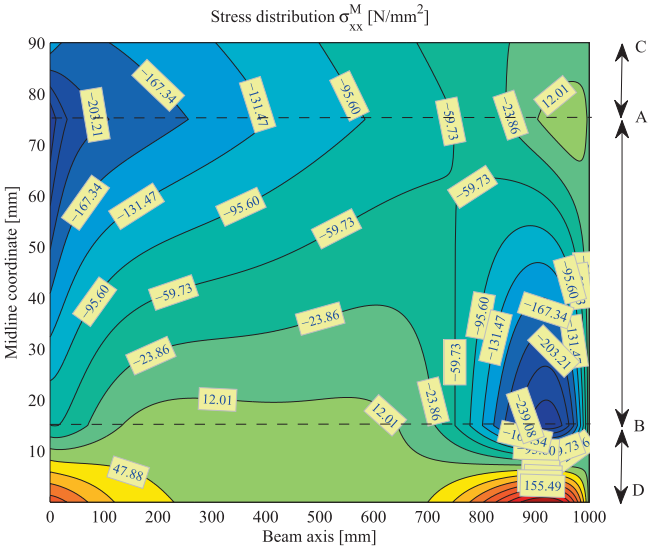

Fig. 35. Stress map of σ^M_{xx} without end stiffener (upper hollow flange – plan view).

An end stiffener restraining all the distortional modes, including not only the nodes displacements but also the displacements of the wall in the direction perpendicular to the wall middle surface, was considered at the end section (where the load is applied), being the membrane stresses for this case represented in Fig. 34; the local warping of the hollow flanges is significantly reduced as can be observed from the patterns of the stress longitudinal distribution.

The membrane stress σ^M_{xs} is also represented for the upper hollow flange in a plan view, Fig. 35, where the concentration of stresses due to the warping can be observed. In Fig. 36 the same stress distribution but for the end stiffener example is presented.

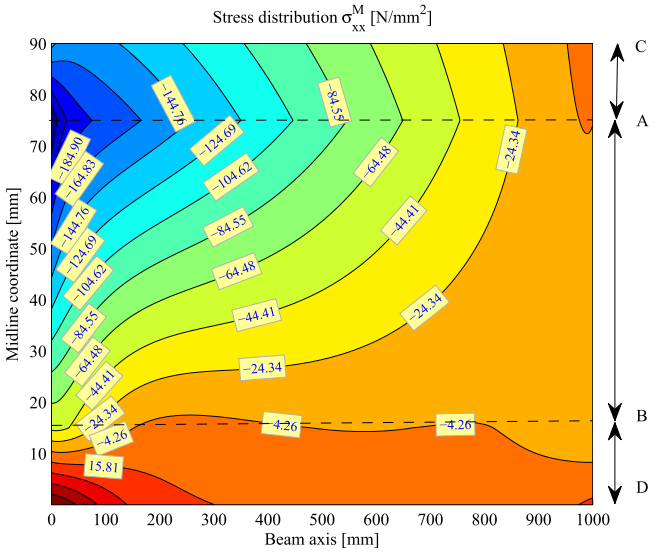

Fig. 36. Stress map of σ^M_{xs} with end stiffener (upper hollow flange – plan view).

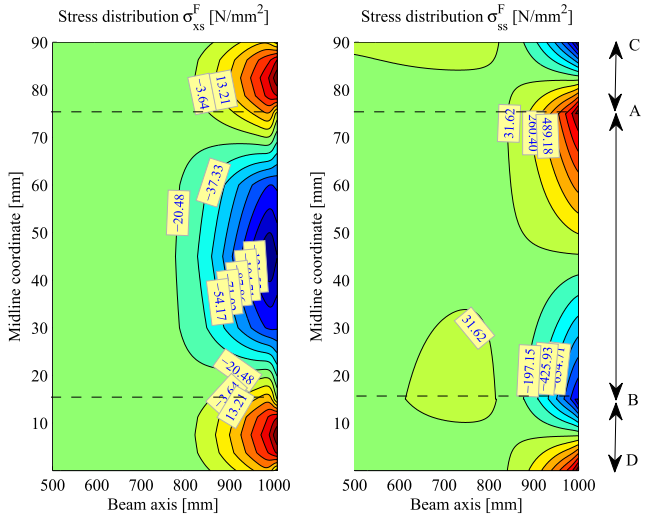

Fig. 37. Transverse flexural stress – upper flange and web.

Table 2
Transverse flexural stress, $\sigma^F_{ss}, N/mm^2$.

	Node **A**	Node **B**
HoBm ($\nu = 0.0,\ \epsilon_{ss} = 0$)	−60.37	55.67
HoBm ($\nu = 0.3,\ \epsilon_{ss} \neq 0$)	−59.08	56.95
Abaqus (S4 elements)	−61.81	56.53

The flexural stresses σ^F_{ss} and σ^F_{xs} in the upper hollow flange (region near the free end) are represented in 37. For comparison purposes, a cross-section analysis considering both the Poisson effect and the transverse extension for the cross-section walls was performed, being the corresponding displacement modes considered in the formulation of the corresponding higher order beam model (an equal mesh of 100 elements was considered). The stresses obtained from both thin-walled beam models (HoBm) are compared with those obtained from the shell finite element model, being the values for the section with an abscissa $x = 800$ mm given in Table 2.

6. Conclusions

A one-dimensional higher order model for the analysis of thin-walled structures with a cross-section profile of a generic polygonal geometry i.e., with an open, closed or branched profile, that considers the warping and the cross-section to be transversely deformable was presented. The model considers a discretization of the cross-section into elements, being the displacement field approximated along the cross-section elements through a set of functions. For each cross-section element an independent approximation is considered for the axial displacements, the tangential displacements along the wall midline direction and the displacements perpendicular to the wall midline.

The displacement field approximation, which is understood as a projection of the displacement on the beam cross-section, allows the enrichment of the solution either by increasing the order of the basis functions adopted or by the refinement of the corresponding support at the beam cross-section level. Such a solution is then capable of representing the thin walled structural behaviour through the definition of non linear cross-section deformation modes that represent three-dimensional elasticity solutions. Due to the unrestricted approximation of the displacement field, the model successfully considers in a "natural" form the shear deformation of the middle surface.

The model formulation is based on the thin-walled governing homogenous differential equation and the associated eigenvalue problem, according to the following steps,

- formulation of the beam differential governing equations and the corresponding eigenvalue problem;
- numerical solution of the quartic eigenvalue problem obtaining,
  - a set of null eigenvalues with an algebraic multiplicity of *twelve* which corresponds to *six* rigid body motion plus *six* classic Saint-Venant solutions, extension, flexure with shear and in the absence of shear in two directions and torsion;
  - a set of eigenvectors associated with the non null eigenvectors representing the higher order solutions of the problem;
- the geometric multiplicity of the null eigenvalue, which is inferior to the corresponding algebraic multiplicity, implies the solution of a Jordan chain procedure, from which a set of fundamental modes, representing the classic Saint-Venant solution as well as shear deformation effects is obtained;
- adopting a Gram-Schmidt procedure, a set of orthogonal basis functions for the displacement field is obtained from the fundamental modes;
- the higher order eigenvectors are filtered from the fundamental basis functions, the result is orthogonalized using a Gram-Schmidt procedure, leading to a set of higher order orthogonal basis functions;
- the sum of the number of fundamental basis functions and the number of higher order basis functions equals the initial number of degrees of freedom in the cross-section displacement approximation;

- a change of basis is considered taking in account a transformation matrix constructed by the fundamental and higher order basis functions, the problem is rewritten in the new set of coordinates;

The eigenvalue problem is solved for the new coordinates, being the same eigenvalues obtained, i.e., the transformation is isospectral, which means that the initial set of equations was not modified during all the process. Moreover, the eigenvalues of a particular deformation mode can be obtained with a reduced model by considering only the relevant displacement modes.

Regarding other beam theories for the analysis of thin-walled structures, the presented higher order model has the advantage of having a general application regarding the cross-section geometry by adopting a unified procedure and also, due to the consistent definition of the corresponding deformation modes through the solution of the respective governing equations, the model allows to accurate represent the three-dimensional behaviour of thin-walled structures. The model has an hierarchic capability that stems from the definition of the corresponding deformation modes, being therefore possible to obtain a reduced model consistent from a structural behaviour perspective.

The higher order model allows to establish a set of uncoupled beam-like equation with a physical interpretation due to the concept and criterion adopting for uncoupling the corresponding deformation modes, being therefore efficient and an alternative to more sophisticated shell finite elements. Some examples have been presented, being the results compared in terms of stresses with the results obtained through a three-dimensional finite element model of shells implemented in Abaqus (2006). The comparison of results is fairly good, in particular if one bears in mind that a one-dimensional model is being compared with a complex three dimensional finite model (Abaqus, 2006). Moreover, the three-dimensional model provides results in terms of stresses not allowing to immediately identify the decomposition of such stresses in terms of the associated structural phenomenon.

Appendix A. Thin-Walled beam coefficient submatrices

The matrices $\mathbf{k}_j^i$ are obtained from the deformation energy functionals as follows: from the functional defined in (24),

$$\mathbf{k}_2^1 = E^* t \int_\Gamma \boldsymbol{\phi} \otimes \boldsymbol{\phi}\, d\Gamma \quad \mathbf{k}_1^1 = E^* \nu t \int_\Gamma \boldsymbol{\phi} \otimes \boldsymbol{\psi}_{,s}\, d\Gamma \quad \mathbf{k}_4 = \frac{E^* t^3}{12} \int_\Gamma \boldsymbol{\chi} \otimes \boldsymbol{\chi}\, d\Gamma \quad \mathbf{k}_2^2 = \frac{E^* \nu t^3}{12} \int_\Gamma \boldsymbol{\chi} \otimes \boldsymbol{\chi}_{,ss}\, d\Gamma$$

from the functional defined in (27),

$$\mathbf{k}_1^3 = G t \int_\Gamma \boldsymbol{\psi} \otimes \boldsymbol{\phi}_{,s}\, d\Gamma \quad \mathbf{k}_2^4 = G t \int_\Gamma \boldsymbol{\psi} \otimes \boldsymbol{\psi}\, d\Gamma$$

$$\mathbf{k}_2^5 = \frac{G t^3}{6} \int_\Gamma \boldsymbol{\chi}_{,s} \otimes \boldsymbol{\chi}_{,s}\, d\Gamma$$

and from the functional defined in(30),

$$\mathbf{k}_0^1 = E^* t \int_\Gamma \boldsymbol{\psi}_{,s} \otimes \boldsymbol{\psi}_{,s}\, d\Gamma \quad \mathbf{k}_1^2 = E^* \nu t \int_\Gamma \boldsymbol{\psi}_{,s} \otimes \boldsymbol{\phi}_{,s}\, d\Gamma$$

$$\mathbf{k}_0^2 = \frac{E^* t^3}{12} \int_\Gamma \boldsymbol{\chi}_{,ss} \otimes \boldsymbol{\chi}_{,ss}\, d\Gamma \quad \mathbf{k}_2^3 = \frac{E^* \nu t^3}{12} \int_\Gamma \boldsymbol{\chi}_{,ss} \otimes \boldsymbol{\chi}\, d\Gamma$$

References

Abaqus, 2006. Abaqus. SIMULIA Dassault Systèmes.

Ádány, S., Schafer, B.W., 2008. A full modal decomposition of thin-walled, single-branched open cross-section members via the constrained finite strip method. Journal of Constructional Steel Research 64 (1), 12–29.

Ádány, S., Silvestre, N., Schafer, B.W., Camotim, D., 2009. GBT and cFSM: two modal approaches to the buckling analysis of unbranched thin-walled members. International Journal of Advanced Steel Construction 5 (2), 195–223.

Andreassen, M.J., Jönsson, J., 2012. Distortional solutions for loaded semi-discretized thin-walled beams. Thin-Walled Structures 50 (1), 116–127.

Andreassen, M.J., Jönsson, J., 2013. A distortional semi-discretized thin-walled beam element. Thin-Walled Structures 62 (4), 142–157.

Antman, S., 1984. Mechanics of Solids, vol. 2. Springer-Verlag.

Bauchau, O., 1985. A beam theory for anisotropic materials. Journal of Applied Mechanics 52, 416–422.

Bazant, Z., 1968. Pièces longues a voiles Épais et calcul des poutres a section déformable. Annales des Ponts et des Chaussées III, 155–169.

Bazant, Z., El Nimieri, M., 1974. Stifness method for curved box girder at initial stress. Journal of Structural Division 100 (ST10), 2071–2090.

Benscoter, S., 1954. A theory of torsion bending for multicell beams. Journal of Applied Mechanics 53, 25–34.

Boswell, L., Zhang, S., 1984. The effect of distortion in thin-walled box spine beams. International Journal of Solids and Strucutres 20, 845–862.

Braun, M., 1993. Differential Equations and Their Applications: An Introduction to Applied Mathematics. Texts in Applied Mathematics, vol. 11. Springer.

Carrera, E., Giunta, G., 2010. Refined beam theories based on a unified formulation. International Journal of Applied Mechanics and Engineering 2, 117–143.

Carrera, E., Petrolo, M., 2011. On the effectiveness of higher-order terms in refined beam theories. Journal of Applied Mechanics 78 (2), 17 pages.

Carrera, E., Giunta, G., Petrolo, M., 2011. Beam Structures: Classical and Advanced Theories. John Wiley and Sons Ltd.

Cowper, G., 1966. The shear coefficient in Timoshenko's beam theory. Journal of Applied Mechanics, 335–340.

Dezi, L., Mentrasti, L., 1985. Nonuniform bending-stress distribution (shear-lag). Journal of Structural Engineering 111 (12), 2675–2690.

Dinis, P., Camotim, D., Silvestre, N., 2006. GBT formulation to analyse the buckling behaviour of thin-walled members with arbitrarily branched open cross-sections. Thin-Walled Structures 44 (1), 20–38.

Fatmi, R.E., 2007. Non-uniform warping including the effects of torsion and shear forces. Part I: A general beam theory. International Journal of Solids and Structures 44 (18–19), 5912–5929.

Flügge, Marguerre, 1948. Wolbkrafte in dünnwandigen profilstäben (Warping in thin-walled beams). Ingenieur-Archiv, 23–38.

Foutch, D., Chang, P., 1982. A shear-lag anomaly. Journal of the Structural Division 108 (ST7), 1653–1659.

Giavotto, V., Borri, M., Mantegazza, P., Ghiringheli, G., 1983. Anisotropic beam theory and applications. Computers and Structures 18, 403–413.

Goheberg, I., Lancaster, P., Rodman, L., 1982. Matrix Polynomials. Academic Press.

Gonçalves, R., 2007. Análise de vigas de parede fina com secão deformável – novas formulações e aplicações. Ph.D. Thesis, TU – Lisbon, Instituto Superior Técnico (in Portuguese).

Gonçalves, R., Dinis, P.B., Camotim, D., 2009. GBT formulation to analyse the first-order and buckling behaviour of thin-walled members with arbitrary cross-sections. Thin-Walled Structures 47, 583–600.

Gonçalves, R., Corrâa, M.R., Camotim, D., 2010. A new approach to the calculation of cross-section deformation modes in the framework of generalized beam theory. Computational Mechanics 46, 759–781.

Haakh, A.H., 2004. Die Erweiterung der VTB für allgemeine dünnwandige Querschnitte sowie die Lösung des Differentialgleichungssystems mit Potenzreihen. Ph.D. Thesis, TU – Darmstadt (in German).

Horgan, C., 1989. Recent developments concerning Saint-Venant's principle: an update. Applied Mechanics Review 42 (11), 295–303.

Hsu, Y., 1995. Ebef method for distortional analysis of steel box girders bridges. Journal of Structural Engineering 121 (3), 557–565.

Jönsson, J., Andreassen, M.J., 2011. Distortional eigenmodes and homogeneous solutions for semi-discretized thin-walled beams. Thin-Walled Structures 49 (6), 691–707.

Kermani, B., Waldron, P., 1993. Analysis of continuous box girder bridges including the effects of distortion. Computers and Structures 47 (3), 427–440.

Kim, J.H., Kim, Y.Y., 1999a. Analysis of thin-walled closed beams with general quadrilateral cross-sections. Journal of Applied Mechanics 66, 904–912.

Kim, J.H., Kim, Y.Y., 1999b. Thin-walled closed box beam element for static and dynamic analysis. International Journal For Numerical Methods in Engineering 45, 473–490.

Kim, J.H., Kim, Y.Y., 2000. One dimensional analysis of thin-walled closed beams having general cross-sections. International Journal For Numerical Methods in Engineering 49, 653–668.

Kim, Y.Y., Kim, Y., 2002. A one-dimensional theory of thin-walled curved rectangular box beams under torsion and out-of-plane bending. International Journal for Numerical Methods in Engineering 53, 1675–1693.

Kim, Y.Y., Kim, Y., 2003. Analysis of thin-walled curved box beam under in-plane flexure. International Journal of Solids and Structures 40, 6111–6123.

Knowles, J., 1966. On Saint-Venant's principle in the two-dimensional theory of elasticity. Archives for Rational Mechanics and Analysis 21, 1–22.

Kuzmanovic, B., Graham, H., 1981. Shear-lag in box girders. Journal of Structural Division 107 (ST9), 1701–1712.

Ladevèze, P., Sanchez, P., Simonds, J., 2003. Beamlike (Saint-Venant) solutions for fully anisotropic elastic tubes of arbitrary closed cross section. International Journal of Solids and Structures 41, 1925–1944.

Lancaster, P., 2005. Isospectral vibrating systems. Part 1. The spectral method. Linear Algebra and its Applications 409, 51–69.

Lancaster, P., Prells, U., 2006. Isospectral families of high-order systems. Tech. Rep., University of Calgary.
Laudiero, F., Savoia, M., 1990. Shear strain effects in flexure and torsion of thin-walled beams with open or closed cross-section. Thin-Walled Structures 10, 87–119.
Li, Z., Hanna, M.T., Ádány, S., Schafer, B.W., 2011. Impact of basis, orthogonalization, and normalization on the constrained finite strip method for stability solutions of open thin-walled members. Thin-Walled Structures 49 (9), 1108–1122.
Mikkola, M., Paavola, J., 1980. Finite element analysis of box girders. Journal of the Structural Division 106 (ST6), 1343–1356.
Möller, R., 1982. Zur berechnung prismatischer strukturen mit beliebigem nicht formtreuem querschnitt. Ph.D. Thesis, TU – Darmstadt (in German).
Morandinia, M., Chierichettib, M., Mantegazzaa, P., 2010. Characteristic behavior of prismatic anisotropic beam via generalized eigenvectors. International Journal of Solids and Structures 47 (10), 1327–1337.
Paavola, J., 1990. A study of curved thin-walled girders. Ph.D. Thesis, Helsinki University of Technology.
Park, N.-H., Choi, S., Kang, Y.-J., 2005. Exact distortional behavior and practical distortional analysis of multicell box girders using an expanded method. Computers and Structures 83 (19–20), 1607–1626.
Pavazza, R., 2002. On the load distribution of thin-walled beams subjected to bending with respect to the cross-section distortion. International Journal of Mechanical Sciences 44 (2), 423–442.
Pavazza, R., Blagojević, B., 2005. On the cross-section distortion of thin-walled beams with multi-cell cross-sections subjected to bending. International Journal of Solids and Structures 42 (3–4), 901–925.
Prokic, A., 1996a. New warping function for thin-walled beams. I – Theory. Journal of Structural Engineering 122 (12), 1437–1441.
Prokic, A., 1996b. New warping function for thin-walled beams. II: Finite element method and applications. Journal of Structural Engineering 122 (12), 1443–1452.
Prokic, A., 2002. New finite element for analysis of shear lag. Computers and Structures 80, 1011–1024.
Razaqpur, A., Li, H., 1991. Thin-walled multicell box-girder finite element. Journal of Structural Engineering 117 (10), 2953–2971.
Razaqpur, A., Li, H., 1994. Refined analysis of curved thin-walled multicell box-girder. Computers and Structures 53 (1), 131–142.
Rubin, M., 2003. On the quest for the best Timoshenko shear coefficient. Journal of Applied Mechanics.
Saadé, K., Warzée, G., Espion, B., 2006. Modeling distortional shear in thin-walled elastic beams. Thin-Walled Structures 44, 808–821.
Schardt, R., 1966. Eine erweiterung der technischen biegetheorie zur berechnung prismatischer faltwerke. Der Stahlbau 35, 161–171 (in German).
Schardt, R., 1989. Verallgemeinerte Technische Biegertheorie. Springer-Verlag (in German).
Silvestre, N., Camotim, D., 2002a. First-order generalised beam theory for arbitrary orthotropic materials. Thin-Walled Structures 40, 755–789.
Silvestre, N., Camotim, D., 2002b. Second-order generalised beam theory for arbitrary orthotropic materialss. Thin-Walled Structures 40, 791–820.
Simão, F., 2005. Post-buckling analysis of thin-walled prismatic members in the context of the generalized beam theory. Ph.D. Thesis, CU – Coimbra, Faculdade de Ciências e Tecnologia da Universidade de Coimbra.
Synge, J.L., 1941. The problem of Saint-Venant for a cylinder with free sides. Quarterly of Applied Mathematics 2, 307–317.
Tesar, A., 1996. Shear-lag in the behaviour of thin-walled box bridges. Computers and Structures 59 (4), 607–612.
Tisseur, F., 2000. Backward error and condition of polynomial eigenvalue problems. Linear Algebra Application 309, 339–361.
Tisseur, F., Meerbergen, K., 2001. The quadratic eigenvalue problem. SIAM Review 43 (2), 235–286.
Toupin, R., 1965. Saint-Venant's principle. Archives of Rational Mechanics 18 (2), 83–96.
Umansky, A., 1940. On normal stresses in torsion of an aircraft wing. Tekhnika vozdushnogo flota Aircraft engineering (in Russian).
Vieira, R.F., 2010. A higher order thin-walled beam model. Ph.D. Thesis, TU – Lisbon, Instituto Superior Técnico.
Vieira, R.F., Virtuoso, F., Pereira, E.B.R., 2013. A higher order thin-walled beam model including warping and shear modes. International Journal of Mechanical Sciences 66, 67–82.
Vlassov, V., 1961. Thin-Walled Elastic Beams. Israel Program for Scientific Translations, Jerusalem.
von Kármán, T., Christensen, N., 1944. Methods of analysis for torsion with variable twist. Journal of Aeronautical Sciences 11, 110–124.
Wilkening, J., 2004. An algorithm for computing jordan chains and inverting analytic matrix functions. Tech. Rep., Courant Institute of Mathematical Sciences.
Wright, R., Abdel-Samad Robinson, A., 1968. Bef analogy for analysis of box-girders. Journal of the structural division 94 (ST7), 147–156.
Yu, W., Hodges, D.H., Ho, J.C., 2012. Variational asymptotic beam sectional analysis – an updated version. International Journal of Engineering Science 44 (11–12), 3738–3755.